Separation and Purification Technology 319 (2023) 123967

Contents lists available at ScienceDirect

Separation and Purification Technology

journal homepage: www.elsevier.com/locate/seppur

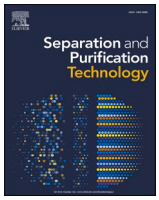

Mechanistic insight into $SO_4^{\bullet-}$/$^{\bullet}OH$ radical for enhancing stability and activity of $LaMO_3$ perovskite toward detoxification of bulk pharmaceutical wastewater: Stoichiometric efficiency and controlled leaching study

Arvind Kumar [a,b,*], Basheswar Prasad [b], Sheena Kumari [a], Faizal Bux [a]

[a] Institute for Water and Wastewater Technology, Durban University of Technology, P.O. Box 1334, Durban 4000, South Africa
[b] Department of Chemical Engineering, Indian Institute of Technology Roorkee, Roorkee 247667, Uttarakhand, India

ARTICLE INFO

Keywords:
Ofloxacin
$LaCoO_3$/PMS system
Perovskite
Phytotoxicity
Pharmaceutical contaminants
Reactive oxygen species

ABSTRACT

This study aims to investigate the detoxification of real pharmaceutical manufacturing wastewater by PMS activated with perovskite $LaMO_3$ (M = Cu, Co, Fe), synthesized by citric sol–gel method. The textural properties of synthesized perovskite were monitored by BET, FESEM/EDS, TEM, XRD, FTIR, and XPS techniques. The effects of key parameters (PMS dose, catalyst, pH and reaction temperature) on ofloxacin degradation along with PMS utilization efficiency as well as PMS consumption were evaluated in detail. Catalyst $LaCoO_3$ exhibited the excellent catalytic activity and stability towards the degradation of ofloxacin (97.11 %) and COD (79.41 %) at optimum operating conditions. Removal of ofloxacin and COD were suppressed by 7 % and 9 % over the fourth cycle, along with minor leaching of Co were observed. Quenching experiments and EPR results demonstrated that both ROS species ($SO_4^{\bullet-}$ and $^{\bullet}OH$) were dominant species for ofloxacin degradation in $LaCoO_3$/PMS system. The treatment cost for ofloxacin degradation in $LaCoO_3$/PMS system was estimated to be 40.78$/m^3 of real pharmaceutical wastewater. Six plausible degradation pathways of ofloxacin were proposed based on intermediate compounds identified by GC-MS and reported literature.

1. Introduction

In the last two decades, the generation of wastewater from pharmaceutical manufacturing has gained a high pace leading to the enormous generation of emerging pollutants in aquatic media [1,2]. These emerging pollutants include various drugs groups viz., antibiotics, steroidal hormones, anti-inflammatory agents, and blood-lipid regulators [3]. The pharmaceutical pollutants enter into aquatic environment by various routes such as directly from production plant and indirectly through anthropogenic activity viz., sewage discharge, landfill leachate, and bleeding, in the presence of surface as well as ground water [1,4]. Prolonged exposure of these pollutants even at low concentration in ng/L to μg/L leads to irreversible and chronicle changes in the microorganism genome and behavior of aquatic organisms [5]. The United States Environmental Protection Agency (USEPA) reported the average daily wastewater generated from pharmaceuticals manufacturing is estimated to be 1.0068×10^9 L [2,6]. Owing to the enormous volume of wastewater generation from pharmaceuticals manufacturing, Indian Environment Ministry has classified pharmaceuticals manufacturing as a red category activity [7]. India is the third largest producer of pharmaceutical in the word after North America and Europe [2]. Among the antibiotics, ofloxacin (OFLX) ($C_{18}H_{20}FN_3O_4$), is one of the most frequently used synthetic fluorinated quinolone-type antibiotic, which has been widely used to treat various kind of bacterial infections [8,9]. Due to high antibacterial activity, OFLX is known as bio-recalcitrant which stay in aquatic media for a long-time [10]. Various researchers have reported the high concentration of OFLX in water environment, such as urban wastewater treatment plant (1.8 μg/L), hospital wastewater (35 μg/L), sewage water (0.89–31.7 μg/L) and surface water (0.5 μg/L) and others work reported in Table 1 [8,11]. Due to potential toxicity, high persistency and low biodegradability, the conventional biological treatment is ineffective for treating such type of pollutants [12,13]. During the last decade, pharmaceuticals manufacturing wastewater and their contaminants particularly OFLX have been treated by various conventional processes including photodegradation [8,11], ozonation, electrochemical degradation [10], sono-photocatalysis [14], adsorption, biological methods [15], and advanced oxidation processes [16], among others work have been reported in Table S6 (supporting

* Corresponding author at: Department of Chemical Engineering, Indian Institute of Technology Roorkee, Roorkee 247667, Uttarakhand, India.
E-mail address: ArvindK@dut.ac.za (A. Kumar).

https://doi.org/10.1016/j.seppur.2023.123967
Received 23 February 2023; Received in revised form 22 April 2023; Accepted 26 April 2023
Available online 2 May 2023

file). However, they have some drawback, for example, adsorption and electrochemical produce a large volume of sludge which causes secondary pollution, and biological processes are very slow in nature [17,18]. Therefore, considering the aforementioned approaches, PMS based AOP's with perovskite catalysts have been proposed for the detoxification of ofloxacin in pharmaceutical wastewater. PMS based AOPs have attracted enormous attention in environmental remediation specially for the degradation of toxic pollutants from aquatic media due to their attractive features such as high oxidation potential of sulfate radical and longer half-life ($SO_4^{\bullet-}$, 2.5–3.1 eV; half-life, 30–40 μs) than hydroxyl radical ($^{\bullet}OH$, 1.8–2.7 eV; half-life 20 μs) along with higher selectivity under wide range of pH [19,20]. Sulfate radicals are mainly generated from PMS or peroxydisulfate (PDS) activation [21]. PMS is more susceptible than PDS to the activation of transition metals due to asymmetric structure ($HO\text{-}O\text{-}SO_3^-$) and longer bond length 1.326 A° [22]. PMS could be easily activated by transition metal ions [23,24], thermolysis [25], ultrasound [26], photocatalysis [27,28] and carbon materials [29]. The use of catalysts can further enhance the efficiency of PMS activation. Perovskite emerged as an attractive materials of mixed oxide family, have been reported to exhibited excellent catalytic activity when activated by PMS for efficient removal of toxic pollutant from wastewater owing to their attractive properties including high electrical conductivity, structural stability and excellent redox property [30–32]. ABO_3 is the general formula of perovskite structure, where A-site occupied by ions of lanthanum or alkaline earth metals and B-site ions occupied by transition metals [33,34]. Perovskite catalysts exhibited outstanding catalytic activity in various areas viz., catalysis with PMS activation, chemical sensor, fuel cell materials and electrochemical etc., [18,23,35–37]. Recently, different types of perovskite like catalyst have demonstrated excellent catalytic activity for the degradation of refractory and highly toxic pollutants in aqueous media such as phenol treated with $ACoO_3$(A = La, Sr, Ce, and Ba) [31], atrazine treated with $LaFe_{1-x}Cu_xO_{3-\Delta}$ perovskite [24], Hydroxybenzoic acid treated with $LnMO_3$ (M = Fe, Co; Ln = La, Pr) [38], and acrylonitrile treated with $La_{0.5}Ce_{0.5}MO_3$ [18] among others reported in supplementary file (Table S7). Various transition metals (Cu, Fe, Co, Ni, Mn) have been employed in B-site cations of lanthanum-based perovskite catalyst and have shown excellent catalytic activity and stability towards PMS activation for addressing the organic contaminants in wastewater. Therefore, to enhance the catalytic activity and stability of catalyst, heterogeneous catalysis with perovskite catalyst $LaMO_3$ (M = Cu, Co, Fe) activated by PMS has been proposed for efficient degradation of ofloxacin in pharmaceutical manufacturing wastewater. To our knowledge, there has been no investigation to date of the degradation of OFLX by heterogeneous catalysis with perovskite catalyst $LaMO_3$ (M = Cu, Co, Fe) activated by PMS so far.

The present study assessed the effects of B site substituted metal ions on PMS activation performance for ofloxacin degradation from real pharmaceuticals manufacturing wastewater utilizing $LaMO_3$ (M = Cu, Co, Fe) perovskites synthesized using a citric sol–gel method. The textural properties of catalyst were monitored by different analytical techniques e.g., BET, FESEM/EDAX, TEM, XRD, FTIR, and XPS. Moreover, the influences of some key parameters such as, PMS dose, catalyst dose, pH and reaction temperature were analyzed for the removal of ofloxacin and COD from pharmaceutical wastewater along with evaluated the PMS utilization efficiency as well as PMS consumption were systematically elucidated in $LaMO_3$/PMS system. In addition, a phytotoxicological study was conducted to assess the toxicity of pharmaceutical manufacturing wastewater on various plant species. Using scavenger and EPR studies, the process of radical generation and evolution were further investigated. Lastly, reusability and stability of the catalyst were evaluated as well as the economic assessment of treatment process.

2. Experimental section

2.1. Chemical reagents used and wastewater collection

All the chemicals used in the study were of analytical reagent grade and detailed discussion available on the supplementary file (Text S1). The wastewater sample were collected from the equalization tank of the effluent treatment plant (ETP) of bulk pharmaceutical manufacturing plant near Saharanpur region Utter Pradesh, India. The collected sample was stored at 4 °C in dark place to prevent the prevent microbial growth and biodegradation. In this study, pure Milli-Q water was used throughout.

2.2. $LaMO_3$ (M = Cu, Co, Fe) perovskite synthesis

Perovskite catalysts $LaMO_3$ (M = Cu, Co, Fe) were prepared through sol–gel method with citric acid (used as a complex agent) employing high grade metal nitrates according to previous literature [34,39]. In a typical synthesis, the precursor solution was prepared by mixing of $La(NO_3)_3{\cdot}6H_2O$, $Fe(NO_3)_3{\cdot}9H_2O$, $Co(NO_3)_2{\cdot}6H_2O$, $Cu(NO_3)_2{\cdot}3H_2O$ and citric in Milli-Q water to form homogeneous solution as shown in the schematic diagram Fig. 1(a). The molar ratio of total metal nitrates to citric acid was maintained as unity (citric acid/(La + M) = 1 where, (M = Cu, Co, Fe)). After stirring vigorously for 12 h with continuous heating at 55 °C, solution was concentrated and became a viscous gel. The viscous gel was further dried at 100 °C for 16 h to get the cake. Subsequently, cake was grinded and calcined in two step, pre-calcined at 350 °C for 2 h followed by final calcined at 700 °C for 5 h. The obtained products were store in desiccator in ambient temperature. The resulting products were designated as $LaCoO_3$, $LaCuO_3$, and $LaFeO_3$ perovskite.

2.3. Catalytic activity measurements

In order to detoxification of pharmaceutical manufacturing wastewater, all the experiments were conducted in a batch reactor (250 mL glass reactor) with a magnetic stirrer, water bath, and total reflux condenser fitted on the top of reactor to preventing the pollutant vapor.

Table 1
Characteristics of the wastewater collected from pharmaceutical drug manufacturing plant.

Parameters		References						
	This study	Patidar et al., 2021	Olevera et al., 2021	Changotra et al., 2019	Malik et al., 2019	Bansal et al. 2018	Gosu et al., 2014	Melero et al., 2009
pH	**7.3**	7.6	–	12.8	8	5.07	6.36	5.6
BOD (mg/L)	**–**	250	218	21,560	250	830	700	381
COD (mg/L)	**1765**	2350	1253.3	37,410	1390	4800	2500	1901
BOD/COD ratio	**–**	0.11	–	0.17	0.18	0.17	0.28	–
TOC (mg/L)	**462.2**	–	431.5	8250	520	–	771.4	860
TDS (mg/L)	**826.3**	1102	–	21,340	1550	1320	–	–
Nitrate (mg/L)	**8.6**	0.35	5.65	18	54	20	3.74	500
Sulfate (mg/L)	**27.5**	–	–	3920	102	526	25.68	–
Ofloxacin (mg/L)	**18.64**	–	–	–	–	–	–	–

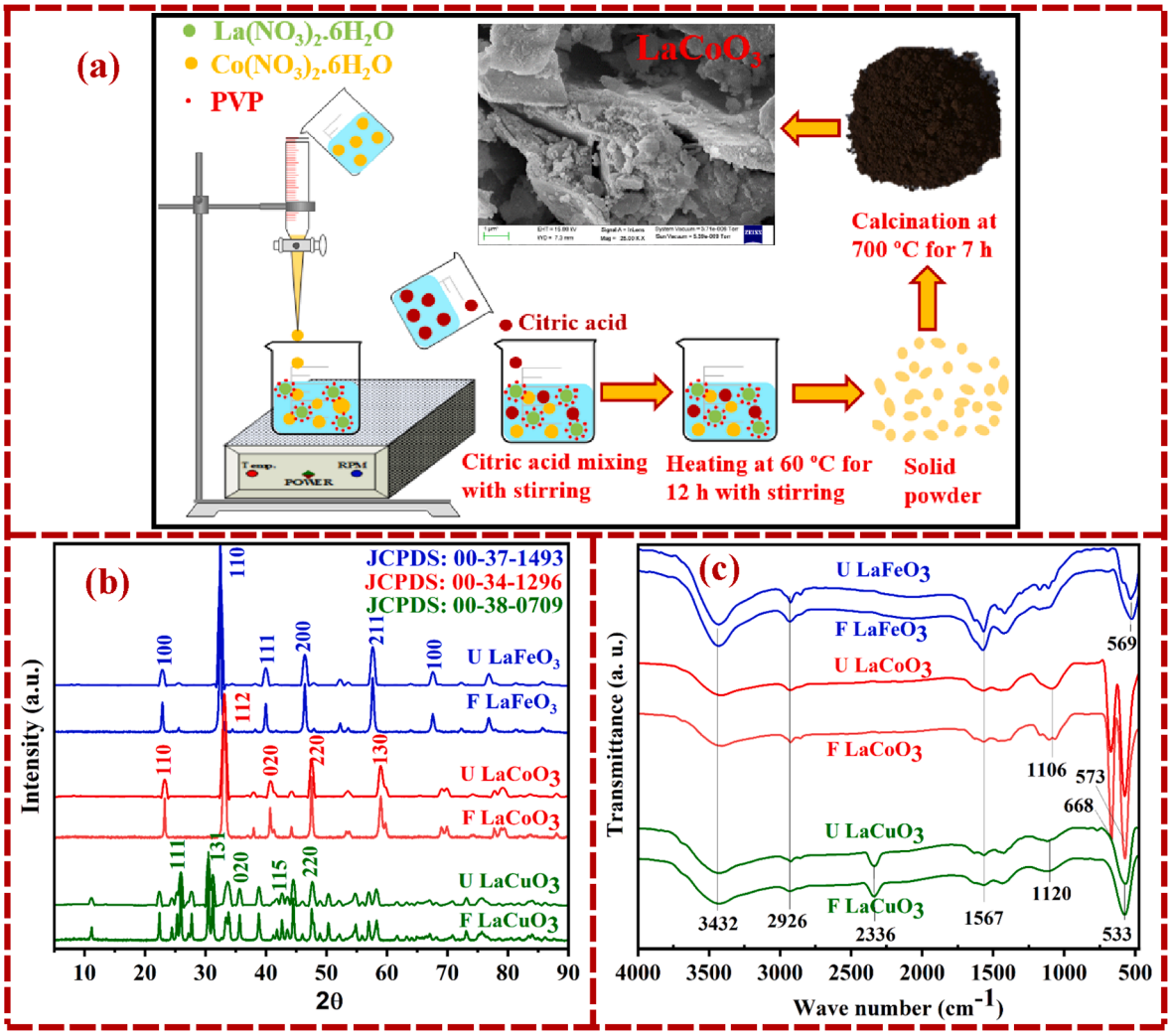

Fig. 1. (**a**) Schematic diagram of $LaMO_3$ (M = Cu, Co, Fe) perovskite catalyst synthesis by sol–gel method,(**b**) XRD spectra, and (**c**) FTIR spectra of fresh and used $LaCuO_3$, $LaCoO_3$, and $LaFeO_3$, catalysts, respectively.

The whole system was placed inside a water bath to maintain the desired temperature. Prior to start the reaction, pH of the solution was regulated using 1 N H_2SO_4 or 1 N NaOH, depending on requirements. The degradation reaction was triggered after introducing the appropriate amount of catalyst dose and PMS dose into 100 mL of wastewater. At the designated time intervals, about 2 mL of aliquots were taken out and quickly filtered using PTFE syringe filter (0.22 μm), immediately equal volume of ethanol was quenched to stop the further degradation reaction. All the experiments were performed at least triplicates, data shown in figures representing the average mean of triplicates and error bars represents the standard deviation of three replicates in all figures.

2.4. Analytical methods and instrumentations

All the instrumentation and analytical techniques used in the study are discussed in detailed in the supplementary file text S2.

3. Results and discussion

3.1. Physico-chemical characterization of $LaMO_3$ (M = Cu, Co, Fe) perovskite catalyst

The X-ray diffraction patterns of fresh and used $LaMO_3$ perovskite catalysts were recorded from 20° to 90° to determine their crystalline structure as well as crystalline phases. The diffraction patterns of catalysts $LaFeO_3$, $LaCoO_3$, and $LaCuO_3$ exhibited the perfect perovskite structure as shown in Fig. 1(b). Diffraction patterns located near 2θ values, 22.63°, 32.21°, 39.73°, 46.20°, and 57.45° index to plain (1 0 0), (1 1 0),(1 1 1), (2 0 0), and (2 1 1) exhibited the cubic crystalline structure of $LaFeO_3$ pure perovskite phase and excellent accord with JCPDS PDF #00–37-1493, space group – 221/Pm3m [38,40]. Another diffraction pattern located near 2θ values, 23.23°, 32.88°, 33.29°,40.65°, 47.50° and 58.98° index to plain (1 1 0), ($\bar{1}$1 0), (1 1 2), (0 2 0), (2 2 0), and (1 3 0) attributed to the rhombohedral crystalline structure of pure perovskite phases $LaCoO_3$, (JCPDS PDF #00–34-1296, space group – 167/R3c). Additionally, the diffraction patterns located near 2θ values, 24.3°, 31.11°, 33.16°, and 47.8° corresponding to plain (1 1 1), (1 1 3), (0 2 0), and (2 2 0) exhibited the La_2CuO_4 phase, resulting in a good agreement with JCPDS PDF #00–38-0709, space group – 69/Fmmm [32]. Further the XRD patterns of spent catalysts were similar to those of fresh catalysts. Neither structural changes nor an additional peak was observed in patterns, but only an increase in intensity of the patterns was observed. As a result, it was demonstrated that catalysts such as $LaFeO_3$, $LaCoO_3$, and $LaCuO_3$ can be reuse for the detoxification of pollutants in wastewater. The mean crystallite size of catalysts was determined using Debye-Scherer equation as discussed in detail in supplementary file text S3. The mean crystallite size of synthesized catalysts $LaFeO_3$, $LaCoO_3$, and $LaCuO_3$ was 14.60 nm, 16.53 nm, and 15.34 nm, based on the Scherer equation respectively. Various authors have been reported the

comparable average crystal sizes for $LaFeO_3$, $LaCoO_3$, and $LaCuO_3$ perovskites [31,40,41].

FTIR spectra of fresh and spent $LaMO_3$ (M = Cu, Co, Fe) perovskite catalysts were recorded within the wavenumber ranges 400–4000 cm^{-1} for analyzing the occurrence of functional group as well as surface chemistry of the catalyst. As depicted in Fig. 1(c), FTIR spectral band near about 3432 cm^{-1} existing in all samples was assigned to O–H stretching, and the broadness of spectral peak represents the hydrogen bonding that existed with high strength [42,43]. The spectral band with wavenumber 2926 cm^{-1} represent the –CH stretching in (CH and C–H_2 vibration) [44]. Observation of a unique peak at wavenumber 2336 cm^{-1} in fresh and used in $LaCuO_3$ catalyst has been attributed to CO_2 molecules adsorbed on the catalyst surface [45]. The spectral band observed near about 1567 cm^{-1} is attributed to the C=C stretching vibration mode while the other spectral band at wavenumbers 1106 cm^{-1} and 1120 cm^{-1} represents the stretching mode of C=O due to presence of residual carbon which might be cause of incomplete combustion of organic species [31,46,47]. As metal ions (i.e., La, Cu, Co, Fe) introduced into the composition, the well-established intense spectral band in the range of 500–700 cm^{-1} (533, 569, 573 and 668 cm^{-1}) could be attributed to a combination of metal and oxygen (M−O−M, M−O, M−OH), whereas, M denotes to metals (i.e., La, Cu, Co, Fe) [39,48,49].

The surface morphology and structure of fresh and used $LaMO_3$ (M = Cu, Co, Fe) perovskite catalysts were analyzed by FE-SEM, elemental composition and content of sample were illustrated by EDAX, as shown in Fig. 2(a-c). As indicated in Fig. 2a, the morphology of fresh $LaCuO_3$ perovskite exhibited a porous like structure with interconnected aggregated particles. There was a small change in morphology of spent $LaCuO_3$ catalyst after treatment, with a roughing of the surface and an enhancement of the porosity as shown in (Fig. S1) in supplementary file. Authors Lu et al., Hammouda et al., also noticed the similar morphology for $LaCuO_3$ catalyst [22,31]. The morphology of fresh $LaCoO_3$ catalyst showed closely packed spherical-like irregular particles with hundreds of nanometers sizes as shown in Fig. 2b [32,50]. Following treatment, the morphology of $LaCoO_3$ catalyst significantly changed, showing that closely packed nano-particles were broken down and a porous like morphology was observed with rough surfaces as shown in supporting file (Fig. S1). As shown in Fig. 2c, catalyst $LaFeO_3$ exhibited agglomerated granular particle with an irregular shape and a broken wall like structure [31]. After treatment, large lumped particle in the size of few micrometers were showed as depicted in Fig. S1. The elemental mapping of the fresh $LaMO_3$ (M = Cu, Co, Fe) perovskite catalysts was carried out to identify elemental content and their distribution on its surface. Based on the elemental mapping, the metal ions (Cu, Co, Fe and La) are homogeneously distributed on the catalyst surface as shown in Fig. S1. In addition, EDAX spectra of fresh and used $LaMO_3$ (M = Cu, Co, Fe) perovskite catalyst showed an intense signal of all elements (La, Co, Cu and Fe). The elemental composition (wt.%) was almost close to stoichiometric composition in catalyst sample as inserted table in EDAX micrographs in supporting file (Fig. S1, S2).

The internal morphology as well as crystallographic information of $LaCoO_3$ perovskite was evaluated using TEM micrographs, as shown in Fig. 2. TEM micrograph captured at 10, 50 and 200 nm scales as shown in Fig. 2d demonstrate spherical-like nano-sized particles interconnected among themselves to form a large network system with irregular sizes and uniformly well dispersed particles. These particles are in a rhombohedral shape which was well matched with XRD results and exhibited the pure perovskite phase of $LaCoO_3$. The lattice fringe having interplanar d-spacing 2.86 nm corresponding to crystallographic plane d_{112} = 2.86 nm attributed to rhombohedral crystalline structure of pure perovskite phases $LaCoO_3$, and good agreement with JCPDS PDF #00–34-1296, space group – 167/R-3c). The observed lattice fringes showed the interplanar d-spacing that indicate that lattice of $LaCoO_3$, have neither collapsed nor destroyed when B-site cations occupied by cobalt in perovskite. In addition, the mean average particle size as shown in Fig. 2(e) was determined using image processing software (Image J Software). According to histogram plot (Fig. 2e), the mean average particle size was 9.6 nm, which is consistent with the average crystal size determined by XRD results.

The texture properties e.g., specific surface area and porosity of fresh and used $LaMO_3$ (M = Cu, Co, Fe) perovskite were evaluated by N_2 adsorption–desorption technique as results shown in Table 2. The BET surface area of synthesized perovskite catalysts $LaCuO_3$, $LaCoO_3$ and $LaFeO_3$, was 9.16, 11.36 and 15.27 m^2/g; and the pore volumes were 0.094, 0.098 and 0.107 cm^3/g, respectively. Notably, specific surface area and pore volume of all the catalysts were significantly reduced after oxidation reaction. The surface area of catalysts $LaCuO_3$, $LaCoO_3$, and $LaFeO_3$ decreased to 7.59, 9.65 and 13.58 m^2/g; and pore volume decreased to 0.079, 0.091 and 0.086 cm^3/g, respectively. In several other studies reported the similar range of specific surface area and pore volume of $LaCuO_3$, $LaCoO_3$, and $LaFeO_3$ perovskites [23,31,40]. Various factors may contribute to the reduction in BET surface area and pore

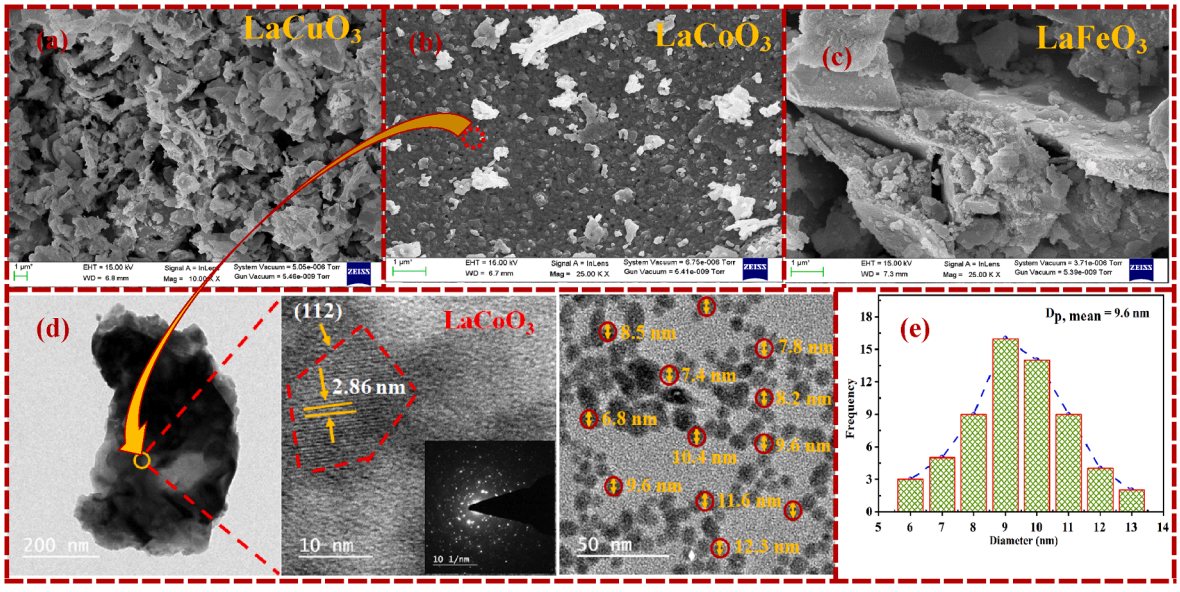

Fig. 2. FE-SEM images of catalysts **(a)** $LaCuO_3$, **(b)** $LaCoO_3$, and **(c)** $LaFeO_3$; TEM micrographs of $LaCoO_3$ catalyst at **(d)** 200 nm,10 nm, and 50 nm, and **(e)** histogram plot of particle size distribution.

Table 2
Textural property of the catalysts.

	FResh catalyst				Spent catalyst		
Catalyst	BET surface area (m^2/g)	Pore volume (cm^3/g)	Pore diameter (nm)	Crystal size(nm)	BET surface area(m^2/g)	Pore volume (cm^3/g)	Pore diameter (nm)
$LaCuO_3$	9.16	0.094	26.59	14.60	7.59	0.079	22.39
$LaCoO_3$	11.36	0.098	31.22	16.53	9.65	0.091	26.36
$LaFeO_3$	15.27	0.107	39.65	15.34	13.58	0.086	34.26

volume of the spent catalysts after treatment. This includes: (**a**) carbon deposition inside the catalyst pores (carbon deposited as in the form of intermediate compounds formed during the reaction) and (**b**) collapse of catalyst pore [43,51,52]. The similar type of decreasing trends has been noticed by authors Zhang et al., and Maghsoodi et al., for $LaMnO_3$ perovskite catalyst [53,54] and Mao et al., for LaCeMn catalyst [51]. The pore diameter of the fresh catalysts $LaCuO_3$, $LaCoO_3$, and $LaFeO_3$ was 26.59 nm, 31.22 nm and 39.65 nm, respectively. After treatment, the

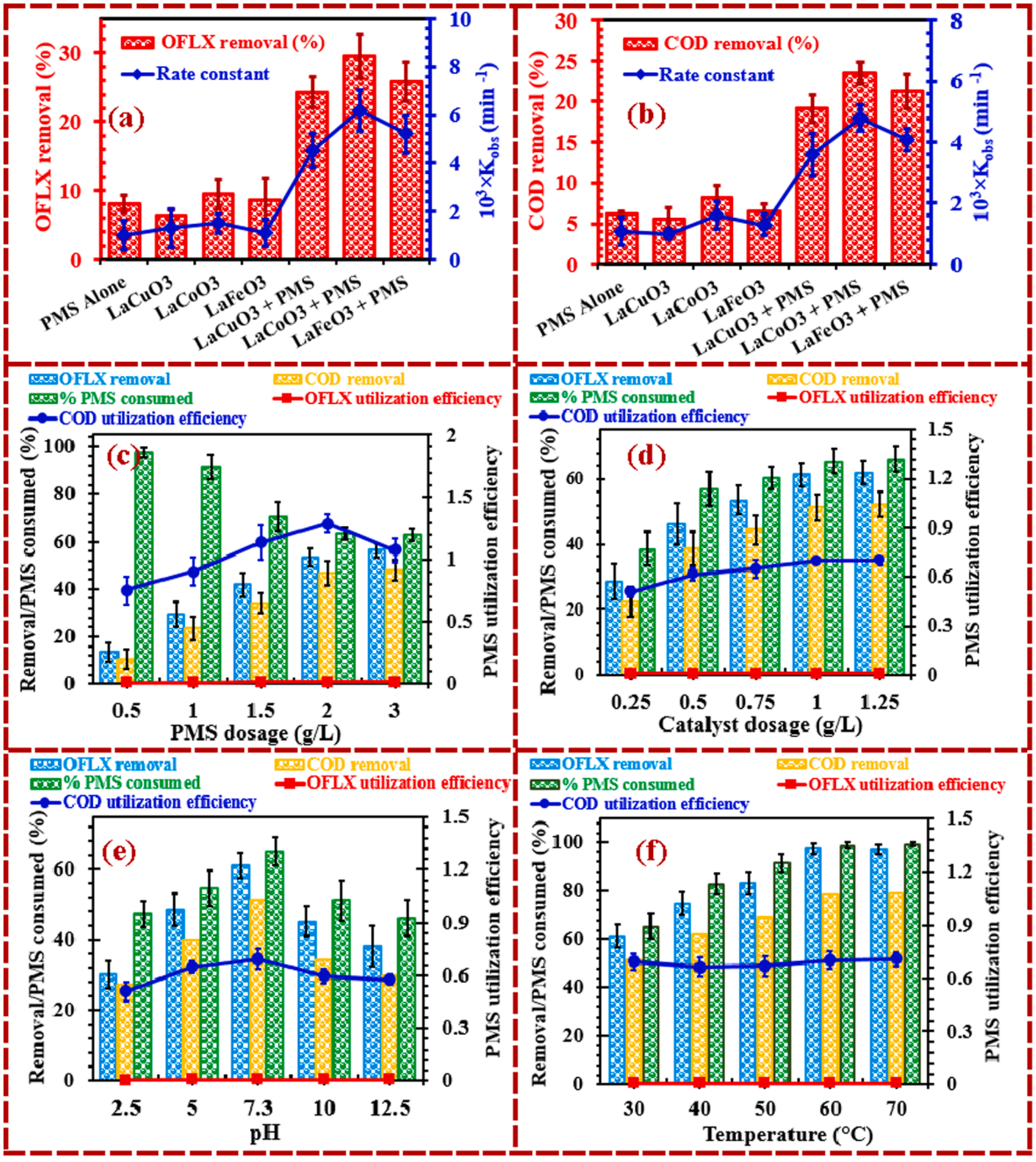

Fig. 3. Preliminary experimental study for **(a)** OFLX and **(b)** COD degradation (**Reaction conditions:** catalysts dose 1 g/L, PMS dose 1 g/L, pH 7.3 and temperature 30 °C); Effects of key parameters on ofloxacin and COD removal: **(c)** effect of PMS dose (catalyst dose 1 g/L, pH 7.3 and temperature 30 °C); **(d)** effect of catalyst dose (PMS dose 2 g/L, pH 7.3 and temperature 30 °C); **(e)** effect of pH (PMS dose 2 g/L, catalyst dose 1 g/L pH 7.3 and temperature 30 °C); and **(f)** effect of reaction temperature (PMS dose 2 g/L, catalyst dose 1 g/L, pH 7.3 and temperature 60 °C).

pore diameter of the spent catalyst was reduced to 22.39 nm, 26.36 nm and 34.26 nm, respectively for $LaCuO_3$, $LaCoO_3$ and $LaFeO_3$.

3.2. Preliminary experimental study for ofloxacin and COD degradation

In order to evaluate the activity of $LaMO_3$ (M = Cu, Co, Fe) catalysts, some preliminary experimental runs were conducted for the degradation of ofloxacin and COD removal from pharmaceutical manufacturing wastewater at room temperature as results depicted in Fig. 3(a, b), and additional details in Fig. S3 and Table S1 in supplementary file. In the control experiment without any catalyst dose, maximum removal of ofloxacin (8.13 %) and COD (6.12 %) were observed while using the 1 g/L PMS alone. This signifies that ofloxacin and COD were challenging to be degraded by PMS alone. The adsorption capacity of $LaCuO_3$, $LaCoO_3$ and $LaFeO_3$ catalysts were individually testified in the absence of PMS, and obtained very low removal efficiency of ofloxacin (i.e., 6.34 %, 9.54 % and 8.69 %) and COD (i.e., 5.62 %, 8.17 % and 6.54 %) under similar reaction conditions (i.e., catalyst dose 1 g/L, natural pH 7.3, temperature 30 °C and 400 rpm stirring speed). However, the above findings indicated that the direct oxidation of ofloxacin by PMS and its adsorption by $LaCuO_3$, $LaCoO_3$ and $LaFeO_3$ catalysts were very minimal. Notably, after adding the catalyst dose and PMS dose into the solution, the degradation of ofloxacin and COD was significantly enhanced. The maximum removal of ofloxacin (i.e., 24.34 %, 29.56 % and 25.78 %) and COD (i.e., 19.17 %, 23.54 % and 21.26 %) achieved under identical conditions with corresponding catalysts $LaCuO_3$, $LaCoO_3$ and $LaFeO_3$. Meanwhile, catalyst $LaCoO_3$ exhibited relatively higher catalytic activity compared to $LaFeO_3$ and $LaCoO_3$ catalyst for the removal of ofloxacin and COD. Therefore, subsequent experiments for ofloxacin and COD removal were conducting using $LaCoO_3$/PMS system.

3.3. Catalytic performance evaluation on ofloxacin and COD degradation

3.3.1. Influence of PMS dose

The Fig. 3(c) illustrate the effects of PMS dosage (0.5–3 g/L) on the degradation of ofloxacin and COD. The degradation of ofloxacin significantly enhanced from 13.57 % to 53.48 % and COD enhanced from 10.4 % to 46.44 % with raising the PMS dose from 0.5 g/L to 2 g/L, at operating conditions (i.e., catalysts dose 1 g/L, natural pH 7.3, reaction temperature 30 °C and reaction time 1 h). With an increase in PMS dose, more ROS species (e.g. $SO_4^{\bullet-}$, $^{\bullet}OH$ and $O_2^{\bullet-}$) were generated which significantly enhanced the degradation of ofloxacin and COD. On contrary, while further increase of PMS dose above 2 g/L, no noticeable changes were observed on ofloxacin and COD removal. This can be attributed to the self-scavenging effect of ROS species and simultaneous production of less oxidizing species like $SO_5^{\bullet-}$ (E° = 1.1 V) which have weaker oxidizing potential compared to species ($SO_4^{\bullet-}$ and $^{\bullet}OH$) and not able to degrade organic pollutants in wastewater as shown via Eq. (1 and 2) [22,24,34].

$$HSO_5^- + SO_5^- \rightarrow SO_5^{\bullet-} + H^+ + SO_4^{2-} \quad (1)$$

$$HSO_5^- + {}^{\bullet}OH \rightarrow SO_5^{\bullet-} + H_2O \quad (2)$$

In order to further confirming the ROS species generation in the $LaCoO_3$/PMS system, residual concentration of PMS was assessed at different PMS dosage (i.e., 0.5, 1, 1.5, 2, and 3 g/L). It could be seen from Fig. 3(c), the consumption of PMS significantly dropped from 97.36 % to 63.42 % when the PMS dose increased from 0.5 g/L to 2 g/L. However, increasing the PMS dosage would enhance the chances of contact between catalyst dose and PMS molecules. While, further increasing the PMS dose from 2 g/L to 3 g/L, no significant changes were observed in PMS consumption, as well as a reduction in ofloxacin and COD level. However, the degradation of ofloxacin and COD was weakened at low dosages of PMS, which can be explained by the fact that insufficient number of $SO_4^{\bullet-}$ radicals available for fixed dose of catalyst [55,56]. Despite the extensive study on PMS consumption, only a few attempts have been made to evaluate the PMS utilization for the degradation of ofloxacin and COD. Thus, we evaluated the effectiveness of PMS utilization by employing the utilization efficiency equation at various PMS dose via Eq. (3). PMS utilization efficiency (η_{PMS}) is the ratio of OFLX degraded (mg/L) to PMS consumed (mg/L) [19,39,57].

$$\eta_{PMS} = \frac{\Delta[OFLX]_{Degradation}}{\Delta[PMS]_{Consumption}} \quad (3)$$

Where, Δ[OFLX] indicate ofloxacin degradation (%) and Δ[PMS] indicate PMS consumed (%). With increase PMS doses up to 2 g/L, PMS utilization efficiencies for ofloxacin and COD removal gradually increased; subsequently decreased when PMS doses were increased from 2 g/L to 3 g/L. For ofloxacin and COD degradation, the PMS utilization efficiencies was 0.010, 0.012, 0.015, 0.016 and 0.013 and for COD degradation 0.750, 0.904, 1.137, 1.290, and 1.078, respectively at various PMS dosages 0.5, 1, 1.5, 2 and 3 g/L. In a previous study, Bao et al., reported PMS utilization efficiencies in the range of i.e., 0.2–0.8 for sulfamethoxazole degradation in PMS/$CoFeO_{2.5}$ system [57]. Likewise, several other authors have reported similar ranges of PMS utilization efficiency for the degradation of various pollutants [19,55,56].

3.3.2. Influence of catalyst dose

Catalyst dose is a crucial parameter and a major source of active sites to activate the PMS which leads to the generation of more radicals. Over dose of the catalyst could enhanced the cost of treatment process and create the secondary pollution by producing a high volume of leachate which contains the heavy metal ions [34,58]. Hence, it is vital to optimize the catalyst dose for the treatment of pharmaceutical wastewater. The effects of various catalyst dosages i.e., 0.25, 0.5, 0.75, 1 and 1.25 g/L were evaluated on the removal of ofloxacin and COD as shown in Fig. 3 (d). The removal of ofloxacin and COD gradually increased from (28.56 % to 61.23 %) and (22.32 % to 51.34 %), respectively with raising the catalyst dose from 0.25 g/L to 1 g/L, respectively at the reaction conditions (i.e., PMS dose 2 g/L, natural pH 7.3, reaction temperature 30 °C and reaction time 1 h). By enhancing the catalyst dose, the growing specific surface area and active sites of the catalysts could facilitate the activation of PMS to produce more ROS species, which effectively improves the degradation of ofloxacin and COD removal. However, a further enhancing the catalyst dose from 1 g/L to 1.25 g/L, showed no significant changes on the removal of ofloxacin and COD. However, the degradation of ofloxacin and COD was weakened with over catalyst dosage. This phenomenon may be caused by an over dose of catalyst dose, which may scavenge the generated more free radicals, which suppresses the removal efficiencies [22,24,34]. The consumption of PMS was progressively increased from 38.64 % to 65.31 % with raising the catalyst dose from 0.25 g/L to 1 g/L. The progressive consumption of PMS leads to generation of more free radicals ($SO_4^{\bullet-}$, $HO^{\bullet}$) via the rapidly decomposition of PMS. However, the consumption of PMS was weakened at high dosage of catalyst above 1 g/L, which leads to sluggish the production of free radicals. The PMS utilization efficiencies were observed to be 0.0069, 0.0077, 0.0083, 0.0087, and 0.0076 for ofloxacin; and 0.506, 0.615, 0.649, 0.693 and 0.697 for COD removal with catalyst dosage 0.25, 0.5, 0.75, 1 and 1.25 g/L, respectively. Meanwhile, PMS utilization efficiency increased with an increase in catalyst dose up to 1 g/L catalyst dose, thereafter, no significant changes in ofloxacin and COD utilization efficiency were observed while further increasing the overdose of catalyst above 1 g/L.

3.3.3. Influence of initial pH

Previous studies have reported that the initial pH of the solution would strongly affect the production of free radicals in heterogeneous PMS oxidation system [24,31]. Thus, effects of pH on the removal of ofloxacin and COD were explored with wide range of pH from 2.5 to 12.5 in the $LaCoO_3$/PMS system. As depicted in Fig. 3(e), removal efficiency of ofloxacin and COD rose from pH 2.5 to 7.3 (natural pH), and

subsequently dropped as pH rose to 12.5. The maximum degradation of ofloxacin (61.23 %) and COD (51.34 %) were noticed with highest PMS consumption (65.31 %) at reaction conditions (i.e., 1 g/L catalyst dose, 7.3 natural pH, 2 g/L PMS dose and reaction time 1 h). Meanwhile, the above results prove that the removal efficiency of ofloxacin and COD continuously decreased in both strong acidic and alkaline medium and observed maximum at around neutral pH. The reasons for decreased removal efficiencies in the acidic medium could be explained from the following aspects: (**a**) in the strong acidic medium, a large amount of H^+ ions formed the hydrogen bond along with peroxyl bond (- O - O -) which quench the ROS ($SO_4^{\bullet-}$, $^{\bullet}OH$) and to form the HSO_4^- and H_2O according to reaction Eqs. (4 and 5), [19,58] (**b**) the poor activity of the catalyst in an acidic medium is ascribed to production of $CoOH^+$ complex, which limits the production of $SO_4^{\bullet-}$ and excessive H^+ ions stabilized with HSO_4^- as shown via Eqs. (6 and 7), which were adversely effects on PMS activation [59]; (**c**) cobalt leaching in strong acidic medium leads to decrease removal efficiency [60,61].

$$H^+ + SO_4^{\bullet-} + e^- \rightarrow HSO_4^- \quad (4)$$

$$H^+ + {}^{\bullet}OH + e^- \rightarrow H_2O \quad (5)$$

$$Co^{+2} + H_2O \rightarrow CoOH^+ + H^+ \quad (6)$$

$$HSO_5^- + SO_4^{\bullet-} \rightarrow SO_4^{2-} + SO_5^{\bullet-} + H^+ \quad (7)$$

Under strong alkaline medium, (**a**) catalytic activity significantly decreased at alkaline pH (pH greater than 9) which might be cause of production of $Co(OH)_2$ precipitate on the catalyst surface and covered the active sites [59,62]; (**b**) Another reason might be self-decomposition of PMS (HSO_5^-) transform into SO_5^{2-} without producing the $SO_4^{\bullet-}$ as shown via Eqs., (8–10). However, SO_5^{2-} a lower oxidation potential than $SO_4^{\bullet-}$ radical, which potentially inhibited the catalytic activity in strong alkaline medium [63,64].

$$HSO_5^- + H_2O \rightarrow SO_5^{2-} + H_3O^+ \quad (8)$$

$$HSO_5^- + SO_5^{2-} \rightarrow HSO_6^- + SO_4^{2-} \quad (9)$$

$$HSO_6^- + SO_5^{2-} \rightarrow HSO_6^- + SO_4^{2-} \quad (10)$$

Notably, the results concluded that neither acidic nor alkaline condition were favorable for ofloxacin degradation in the $LaCoO_3$/PMS system. Herein, PMS utilization efficiency for ofloxacin and COD degradation was evaluated at various pHs (2.5, 5, 7.3, 10, 12.5) as depicted in Fig. 3(e). The PMS utilization efficiencies enhanced from 0.006 to 0.009 for ofloxacin and 0.510 to 0.693 for COD by raising the pH from 2.5 to 7.3, respectively. While further adjusting the pH from 7.3 to 12.5, PMS utilization efficiencies gradually dropped from 0.009 to 0.008 for ofloxacin and 0.693 to 0.574 for COD, respectively. The PMS utilization efficiency results were found to be in agreement with data previously reported by different authors [4,19,55,57].

3.3.4. Influence of reaction temperature

The elevated reaction temperature played a vital role in promoting ofloxacin and COD degradation in $LaCoO_3$/PMS system. Accordingly, the effect of various temperatures ranges 30–70 °C was evaluated on degradation of ofloxacin and COD as results depicted in Fig. 3(f). On increasing the reaction temperature from 30 °C to 60 °C, removal efficiency of ofloxacin and COD significantly increased from (65.31 % to 98.87 %) and (51.34 % to 79.41 %), respectively with an elevating the reaction temperature from 30 ℃ to 60 °C, along with the consumption of PMS simultaneously enhanced from 65.31 % to 98.87 % with elevating reaction temperature from 30 °C to 60 °C. However, further increasing the reaction temperature above 60 °C, no noticeable change on ofloxacin and COD removal were observed and PMS was entirely consumed (99.15 %) at 70 °C. Furthermore, elevating the reaction temperature may result in the progressive formation of ROS species ($SO_4^{\bullet-}$ and $^{\bullet}OH$) as shown in Eq. (11) [39,56]. An asymmetric structure of PMS makes them unstable at high temperature above greater than 60 °C. At high temperature, fission of bond O − O in PMS structure could be easily broken and subsequently accelerate the side reaction Eqs. (12–15), resulting in suppressing the production of ROS ($SO_4^{\bullet-}$ and $^{\bullet}OH$) [65,66]. Additionally, the PMS utilization efficiencies for ofloxacin were observed 0.0087, 0.0083, 0.0085, 0.0091 and 0.0092; and for COD degradation 0.693, 0.663, 0.667, 0.701 and 0.706, at several temperatures i.e., 30, 40, 50, 60 and 70 °C, respectively.

$$HSO_5^- + \text{Heat} \rightarrow SO_4^{\bullet-} + {}^{\bullet}OH \quad (11)$$

$$HSO_5^- + SO_4^{\bullet-} \rightarrow HSO_5^{\bullet-} + H^+ + SO_4^- \quad (12)$$

$$HSO_5^- + {}^{\bullet}OH \rightarrow SO_5^{\bullet-} + H_2O \quad (13)$$

$$SO_4^- + H_2O \rightarrow SO_4^{2-} + {}^{\bullet}OH + H^+ \quad (14)$$

$$2SO_4^- + 2\,{}^{\bullet}OH \rightarrow 2HSO_4^- + O_2 \quad (15)$$

3.4. Identification and detection of free radicals

The identification of dominant ROS species for the removal of ofloxacin and COD in $LaCoO_3$/PMS system were explored by conducting the different quenching experiments as shown in Fig. 4(a, d). According to previous literature, in heterogeneous sulfate radical based AOPs major reactive species namely sulfate radicals ($SO_4^{\bullet-}$), hydroxyl radicals ($^{\bullet}OH$), peroxysulfate radicals ($SO_5^{\bullet-}$), singlet oxygen ($^1O_2$) were generated [19,23,61]. The activity of $SO_5^{\bullet-}$ can be neglected due to its weaker oxidizing ability [64]. It has been thoroughly demonstrated in the literature that ethanol (EtOH) could easily reacts with both $SO_4^{\bullet-}$ ($k = 1.6 \times 10^7 - 7.7 \times 10^7\ M^{-1}s^{-1}$) and $^{\bullet}OH$ ($k = 1.2 \times 10^9 - 2.8 \times 10^9\ M^{-1}s^{-1}$), while *tert*-butyle alcohol (TBA) quickly react with $^{\bullet}OH$ radicals and having much higher rate constant value ($k = 3.8 \times 10^8 - 7.6 \times 10^8\ M^{-1}s^{-1}$) compare to $SO_4^{\bullet-}$ ($k = 4 \times 10^5 - 9.1 \times 10^5\ M^{-1}s^{-1}$). Meanwhile, the rate constant value for $^{\bullet}OH$ radical is 1000 times higher compare to $SO_4^{\bullet-}$ radical [22,39]. Therefore, TBA was chosen as a $^{\bullet}OH$ radical scavenger and ethanol (EtOH) was chosen as a scavenger of both $SO_4^{\bullet-}$ and $^{\bullet}OH$ radical. In addition, L-histidine is a popular scavenger for singlet oxygen ($^1O_2$) [39,65]. As shown in Fig. 4(c, d), 97.11 % of ofloxacin and 79.41 % of COD removal were noticed while no any quencher dose was utilized. After adding the 10 mM of each concentration LH, TBA and EtOH individually into the $LaCoO_3$/PMS system, the removal of ofloxacin suddenly dropped from 97.11 % to 89.91 %, 68.46 %, and 61.76 %; and COD from 79.41 % to 73.25 %, 67.68 %, and 64.48 %, at optimum operating conditions and results shown in Table S2 (in supporting file). Notably, EtOH had a more significant inhibitory effects on ofloxacin and COD removal compared to TBA and LH. Furthermore, the effects of high dosage of EtOH in the range of 10–200 mM were investigated under the same optimum operating conditions. The ofloxacin removal efficiency was potentially suppressed from 61.76 % to 39.92 %, and for COD 64.48 % to 47.6 %, while raising the EtOH dose from 10 mM to 200 mM, respectively. Authors Yan et al., noticed the removal of sulfamethoxazole suppressed more than 52 % and 72 % in the presence of 500 mM EtOH and 500 mM TBA, respectively. Similar trend for carbamazepine degradation was noticed, only 84 % and 15 % of carbamazepine removal efficiency inhibited in the presence of 100 mM TBA and 500 mM EtOH, respectively [21,59]. The value of rate constants was estimated to be $K_{OFLX} = 153.3 \times 10^6\ Lmg^{-1}s^{-1}$ for OFLX and $16.6 \times 10^7\ Lmg^{-1}s^{-1}$ for COD removal in the absence of any scavenger. Furthermore, the values of rate constant for OFLX was estimated (40.2×10^6, 10.8×10^6 and $8.5 \times 10^6\ Lmg^{-1}s^{-1}$) and for COD removal ($15.3 \times 10^7$, 10.6×10^7 and $10.2 \times 10^7\ Lmg^{-1}s^{-1}$) in the presence of 10 mM of each quencher LH, TBA and EtOH, respectively. However, the rate of OFLX and COD removal significantly suppressed from $8.5 \times 10^6\ Lmg^{-1}s^{-1}$ to $3.16 \times 10^6\ Lmg^{-1}s^{-1}$, and $10.2 \times 10^7\ Lmg^{-1}s^{-1}$ to $5.0 \times$

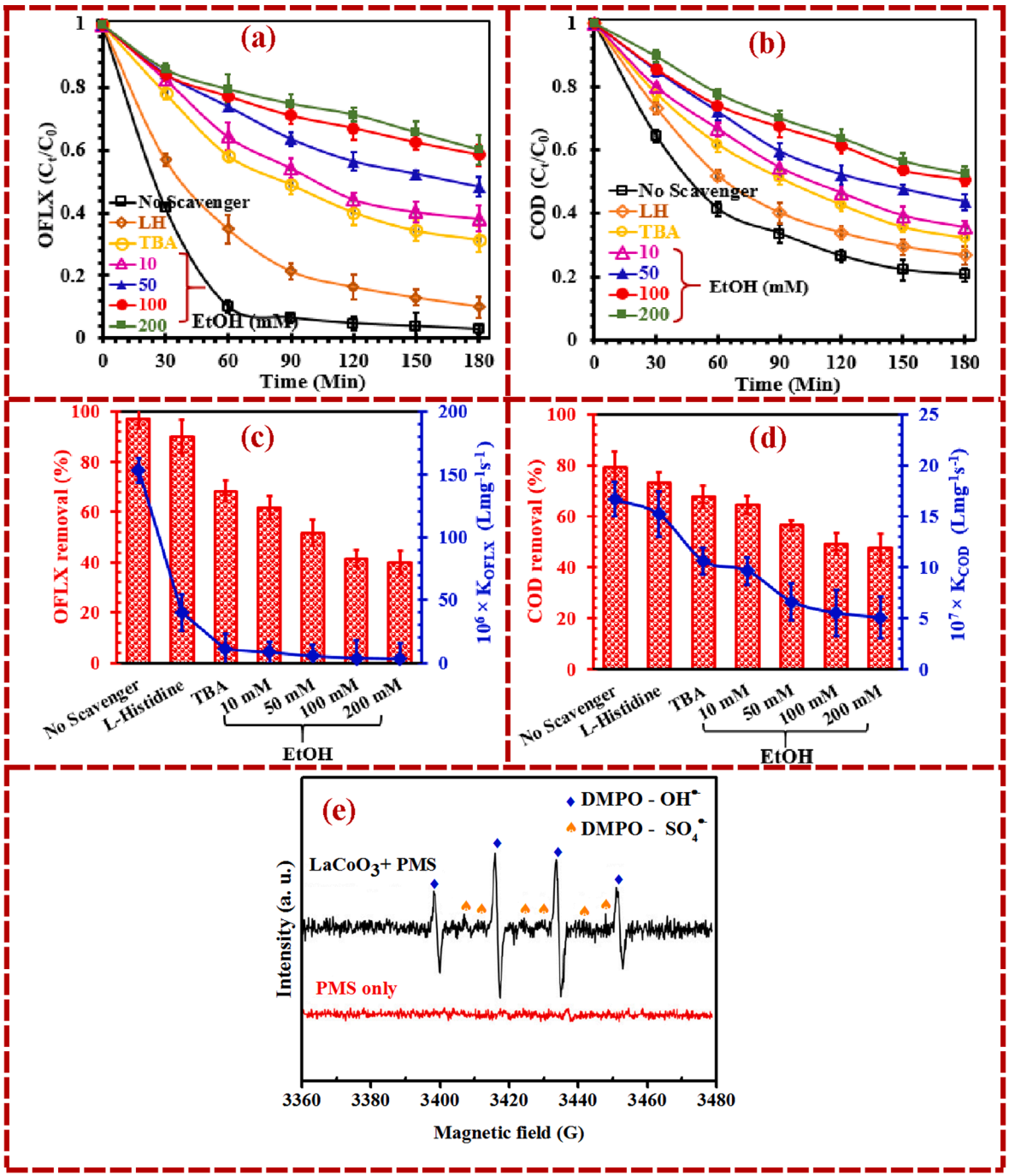

Fig.4. Effects of various scavengers on the degradation of (**a**) ofloxacin, (**b**) COD, with their corresponding inhibition kinetics for (**c**) ofloxacin, (**d**) COD, at optimum operating conditions in the $LaCoO_3$/PMS system, and (**e**) EPR spectra of PMS only and $LaCoO_3$/PMS (**Reaction conditions:** PMS dose 2 mM, catalyst dose 1 g/L, pH 7.3 and temperature 60 °C).

10^7 $Lmg^{-1}s^{-1}$, while raising the EtOH dosage from 10 mM to 200 mM, respectively. The aforementioned results demonstrate that both ROS species i.e., $SO_4^{\bullet-}$ and $^{\bullet}OH$ played a vital role in ofloxacin and COD degradation.

To further confirm the ROS species that is responsible for degradation of ofloxacin, ESR study was conducted with employing the DMPO as the spin-trapping agent at optimum reaction conditions (e.g., PMS dose 2 g/L, $LaCoO_3$ dose 1 g/L, pH 7.3, reaction temperature 60°C) with 10 mM of DMPO. Generally, DMPO was used to trap $SO_4^{\bullet-}$ and $^{\bullet}OH$ radicals with the formation of DMPO-$SO_4^{\bullet-}$ and DMPO-$^{\bullet}OH$. As illustrated in Fig. 4(e), no noticeable signals of DMPO-$SO_4^{\bullet-}$ and DMPO-$^{\bullet}OH$ adducts were identified while using the PMS dose alone, which reveals that no radicals were produced with only the PMS in the absence of catalyst. However, the characteristic signal of DMPO-$SO_4^{\bullet-}$ adduct with hyperfine splitting constants (α_N = 13.6 G, α_H = 9.7 G, α_H = 1.48 G, α_H = 0.78 G) and DMPO-$^{\bullet}OH$ ($\alpha_N = \alpha_H$ = 14.9 G) were strongly observed when the PMS dose and catalyst dose added as depicted in Fig. 4(e), resulting in generation of $SO_4^{\bullet-}$ and $^{\bullet}OH$ radicals. Although, characteristic signal of DMPO-$^{\bullet}OH$ is much stronger in comparison with that of DMPO-$SO_4^{\bullet-}$ which might be cause of the short life-span of DMPO-$SO_4^{\bullet-}$ adduct ($t_{1/2}$ = 95 s in water) and high reaction rate for hydroxyl radical ($k_{DMPO\text{-}^{\bullet}OH}$ = 2.8×10^9 $M^{-1}s^{-1}$) compared to sulfate/sulfide ($k_{DMPO\text{-}SO4^{\bullet-}} = 1.2 \times 10^9$ $M^{-1}s^{-1}$) [4,67]. Adduct DMPO-$SO_4^{\bullet-}$ rapidly transformed into DMPO-$^{\bullet}OH$ through nucleophilic substitution as shown via Eqs. (16–17).

$$DMPO - SO_4^{\bullet -} + H_2O \rightarrow DMPO - {}^{\bullet}OH + SO_4^{2-} + H^+ \quad (16)$$

$$SO_4^{\bullet -} + H_2O \rightarrow {}^{\bullet}OH + SO_4^{2-} + H^+ \quad (17)$$

Authors Lu et al., also noticed the similar findings and reported that both radicals $SO_4^{\bullet -}$ and $^{\bullet}OH$ generated in PMS/$LaCo_{0.4}Cu_{0.6}O_3$ system [22]. All these findings agree with those in aforementioned radical quenching experiments and indicate that both radicals $SO_4^{\bullet -}$ and $^{\bullet}OH$ were generated in PMS/$LaCoO_3$ system.

3.5. Ofloxacin degradation mechanism in $LaCoO_3$/PMS system

3.5.1. PMS activation mechanism

In order to explore the PMS activation mechanism with $LaCoO_3$ perovskite, the XPS spectra of $LaCoO_3$ before and after treatment were recorded as illustrated in Fig. 5(a, d). The full survey scan XPS spectra of $LaCoO_3$ perovskite before and after treatment demonstrated that as synthesized particles are mainly composed of elements i.e., Co (2p), La (3d) and O (1 s) as depicted in Fig. 5(a). The entire spectrum was calibrated using C 1 s peak with binding energy 284.8 eV. As shown in Fig. 5 (b), typical XPS spectra of Co 2p3/2 for fresh $LaCoO_3$ deconvoluted into two peaks at binding energy 774.9 eV and 772.6 eV, which were

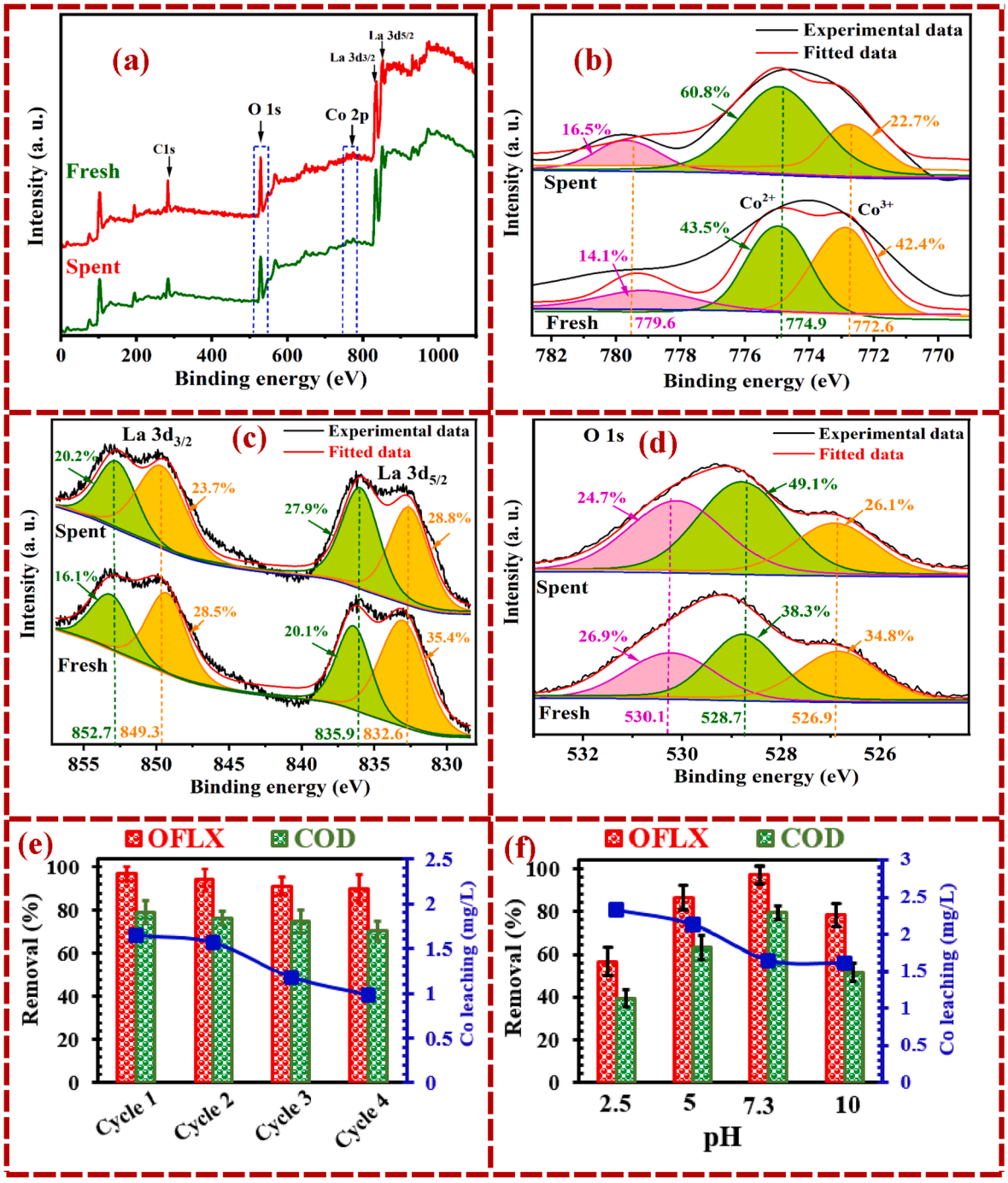

Fig. 5. XPS spectra of fresh and spent $LaCoO_3$ catalyst, (**a**) survey scan spectra, (**b**) Co 2p spectra, (**c**) La 3d spectra, (**d**) O1s spectra, (**e**) reusability study of $LaCoO_3$ catalyst and (**f**) effect of pH with Co leaching, at optimum operating conditions in the $LaCoO_3$/PMS system.

attributed to Co^{+2} (43.5 %) and Co^{+3} (42.4 %) with corresponding composition [22]. After oxidation reaction, a significant change in the composition of Co^{+2} and Co^{+3} was observed, which accounted for 22.77 % and 60.8 % in spent catalyst, respectively. This is clear indication of ions Co^{+2} and Co^{+3} involved in PMS activation via the electron transfer cycle between Co^{+2} and Co^{+3} and to produces the free radicals for the degradation of ofloxacin. Meanwhile, Co^{+3} accept the electron from the system resulting in a redox reaction process i.e., $Co^{+2} \leftrightarrow Co^{+3} \leftrightarrow Co^{+2}$ involved in the PMS oxidation as shown in the following equation Eq. (18) and (19) [22,57,68,69].

$$\equiv Co^{2+} + HSO_5^- \rightarrow \equiv Co^{3+} + SO_4^{\bullet-} + OH^- \quad (18)$$

$$\equiv Co^{3+} + HSO_5^- \rightarrow \equiv Co^{2+} + SO_5^{\bullet-} + H^+ \quad (19)$$

XPS spectra of La 3d core level of fresh $LaCoO_3$ perovskite showed two characteristic peaks of La $3d_{5/2}$ at around binding energy with their corresponding composition i.e., 832.6 eV (35.4 %) and 835.9 eV (20.1 %); and for La $3d_{3/2}$ at around i.e., 849.7 eV (28.5 %) and 852.7 eV (16.1 %), which could be assigned to La^{+3} oxidation state in species La_2O_3 and $La(OH)_3$, respectively [70,71]. Fig. 5(c) showed that after oxidation reaction, no significant changes were observed in binding energy, only the composition had changed. The XPS spectra of O1s core level of fresh catalyst split into three peaks with their corresponding composition namely, lattice oxygen (O_2^{2-}/O^-) at 526.9 eV (34.8 %), surface adsorb oxygen (O_A) at 528.7 eV (38.3 %), and carbonated oxygen at 530.1 eV (26.9 %), respectively. Notably, lattice oxygen composition of spent $LaCoO_3$ catalyst was significantly decreased, which is clear indication of consumption of highly oxidative species ($SO_4^{\bullet-}$ and $^{\bullet}OH$) [24,72]. Moreover, the composition of surface adsorb oxygen increased from 38.3 % to 49.1 %. This might be caused by − OH group in H_2O molecules participating in the PMS activation process and subsequently more − OH groups were formed during the redox process along with Co − OH group were also formed on the catalyst surface [69,73]. Apart from that, no noticeable changes were observed in carbonated oxygen composition.

Based on the aforementioned results obtained from the XPS analysis, quenching experimental study, and EPR tests, we proposed a possible PMS activation mechanism in $LaCoO_3$/PMS system for ofloxacin degradation. The redox conversion of metal ions between M^{n+} and $M^{(n+1)+}$ (M represents transition metal) plays a vital role in PMS activation by fission of -O − O- bond in PMS [22,24]. According to literature, Co ions act as Lewis acid on the catalyst $LaCoO_3$ surface, when the catalyst introduced into the aqueous media, water molecules physically adsorbed the $\equiv Co^{+2}$ sites of catalyst $LaCoO_3$ surface to create $\equiv Co^{+2}$-OH^- Eq. (20), which is rate limiting reaction for PMS activation [73,74]. Subsequently, when PMS was introduced into the reaction solution, PMS (HSO_5^-) was bonded in the form of $LaCoO_3$ − O − H-HSO_5^- through hydrogen bonding. After PMS introduction, formed complex $\equiv Co^{+2}$-OH^- further react with PMS to produce the $SO_4^{\bullet-}$ via hydrogen bonding along with $SO_5^{\bullet-}$ radical species via Eqs. (21–22). Meanwhile, generated radical $SO_5^{\bullet-}$ via Eq. (21, 22) combined with each other produce a small amount of $SO_5^{\bullet-}$ radicals via Eq. (23) [39,69].

$$\equiv Co^{2+} - OH + HSO_5^- \rightarrow \equiv Co^{+3} - OH + SO_4^{\bullet-} + OH^- \quad (20)$$

$$\equiv Co^{3+} - OH + HSO_5^- \rightarrow \equiv Co^{2+} - OH + SO_5^{\bullet-} + H^+ \quad (21)$$

$$\equiv Co^{3+} + HSO_5^- \rightarrow \equiv Co^{2+} + SO_5^{\bullet-} + H^+ \quad (22)$$

$$SO_5^{\bullet-} + SO_5^{\bullet-} \rightarrow 2SO_4^{\bullet-} + O_2 \quad (23)$$

In addition, $OH^{\bullet}$ radicals were also produced in the progressive oxidation reduction cycle $Co^{+2} \leftrightarrow Co^{+3} \leftrightarrow Co^{+2}$ via equation Eq. (24–26). The production of $OH^{\bullet}$ radical is also accompanied by the production of peroxyl radicals ($HO_2^{\bullet}$) which have a lower oxidation potential compared to OH• radical via Eq. (27). Finally, the formed reactive species oxidized the ofloxacin into intermediate compounds which could be further oxidized into CO_2 and H_2O via Eq. (28).

$$\equiv Co^{2+} + HSO_5^- \rightarrow \equiv Co^{3+} + SO_4^{2-} + {}^{\bullet}OH \quad (24)$$

$$H_2O + HSO_5^- \rightarrow HSO_4^- + H_2O_2 \quad (25)$$

$$H_2O_2 \rightarrow 2\ {}^{\bullet}OH \quad (26)$$

$$H_2O_2 + {}^{\bullet}OH \rightarrow {}^{\bullet}OH_2 + H_2O \quad (27)$$

$$Ofloxacin + SO_4^{\bullet-} / {}^{\bullet}OH \rightarrow Intermediates \xrightarrow{Mineralization} CO_2 + H_2O \quad (28)$$

Moreover, the ofloxacin degradation pathways were elucidated through the intermediate compound generated during the reaction as detected by GC-MS in $LaCoO_3$/PMS system as well as from the literature. Overall, thirteen compounds were tentatively identified; details of these compounds such as elemental formula, proposed structure and molecular ions (m/z ratio) were shown in supplementary data (Table S4 and Table S5). Basis on GC-MS analysis and previously reported ofloxacin degradation pathways, six reaction pathways were proposed as shown in Fig. 8 [10,11,14,75,76]. In the proposed pathways, several major transformation mechanisms were described e.g., hydroxylation, piperazinyl dealkylation, decarboxylation, cleavage of OFX molecule, defluorination and oxidation of hydroxyl groups, etc., [8,9,14]. In the first degradation pathways, ofloxacin degradation begins with hydroxylation of the tetrahydropyridine ring and ring cleavage being attacked by $SO_4^{\bullet-}$ and $^{\bullet}OH$ radicals, leading to formation of the product (m/z −397). Apart from that intermediate products (m/z −282) and (m/z −117) were formed by strong attacks of $SO_4^{\bullet-}$ and $^{\bullet}OH$ radicals on C–C bond broken in carboxylic acid and benzene ring. Subsequently, product (m/z −282) could be transformed into the product (m/z − 165) and (m/z − 87) via cleavage of benzene ring by further attacking the reactive radicals. In the second pathways, intermediate products (m/z − 101) and (m/z − 280) were produced through $SO_4^{\bullet-}$ and $^{\bullet}OH$ radicals attacked on C-N bond cleavage between piperazine ring and benzene binding. Thereafter, an intermediate compound (m/z − 133) was formed by the cleavage on piperazine ring of product (m/z − 100) which then further transformed into another product (m/z − 87). Moreover, in 3rd proposed pathway, the cleaved piperazine ring may be attached by reactive species $SO_4^{\bullet-}$/$^{\bullet}OH$ to form the product (m/z − 364), which could be further transformed into product (m/z C 279) via C-N bond cleavage. Subsequently, cleaved benzine ring attacked by $SO_4^{\bullet-}$/$^{\bullet}OH$ to produce product (m/z − 228). In the pathways four, product (m/z − 279) might be formed via oxidative degradation of N-piperazine ring leaving an amino group on the ring. Then product (m/z − 279) may further transform after losing the carbon moiety [11,14]. The products (m/z − 251) and (m/z − 207) were produced after losses of CO and CO_2 from corresponding product (m/z − 279) and (m/z − 251), along with product (m/z − 205) was formed after losing the 2 hydrogen from product (m/z − 207) which leads to formation of one double bond in methyl group. In pathway fifth, product (m/z − 175) was formed by breakdown of parental compound and losing the $C_8H_{13}FN_2O_2$, subsequently, m/z 175 get further transformed by cleavage into product (m/z − 149). At the end of the pathway six, product (m/z − 395) was formed via dihydroxylation of ofloxacin as 2-HO-OFLX. Eventually, detected intermediate products were further oxidized into a smaller compound and it got mineralized into CO_2 and H_2O.

3.6. Recyclability and chemical stability of $LaCoO_3$ perovskite

The recyclability and stability of $LaCoO_3$ perovskite in $LaCoO_3$/PMS system were assessed over the four consecutive cycles under the same optimum operating conditions e.g., PMS dose 2 g/L, $LaCoO_3$ catalyst dose 1 g/L, pH 7.3, and reaction temperature 60 °C, as results depicted in Fig. 5(e) and (Table S3 in supporting file). The removal of ofloxacin and COD was observed 97.11 % and 79.41 % in the first cycle, respectively.

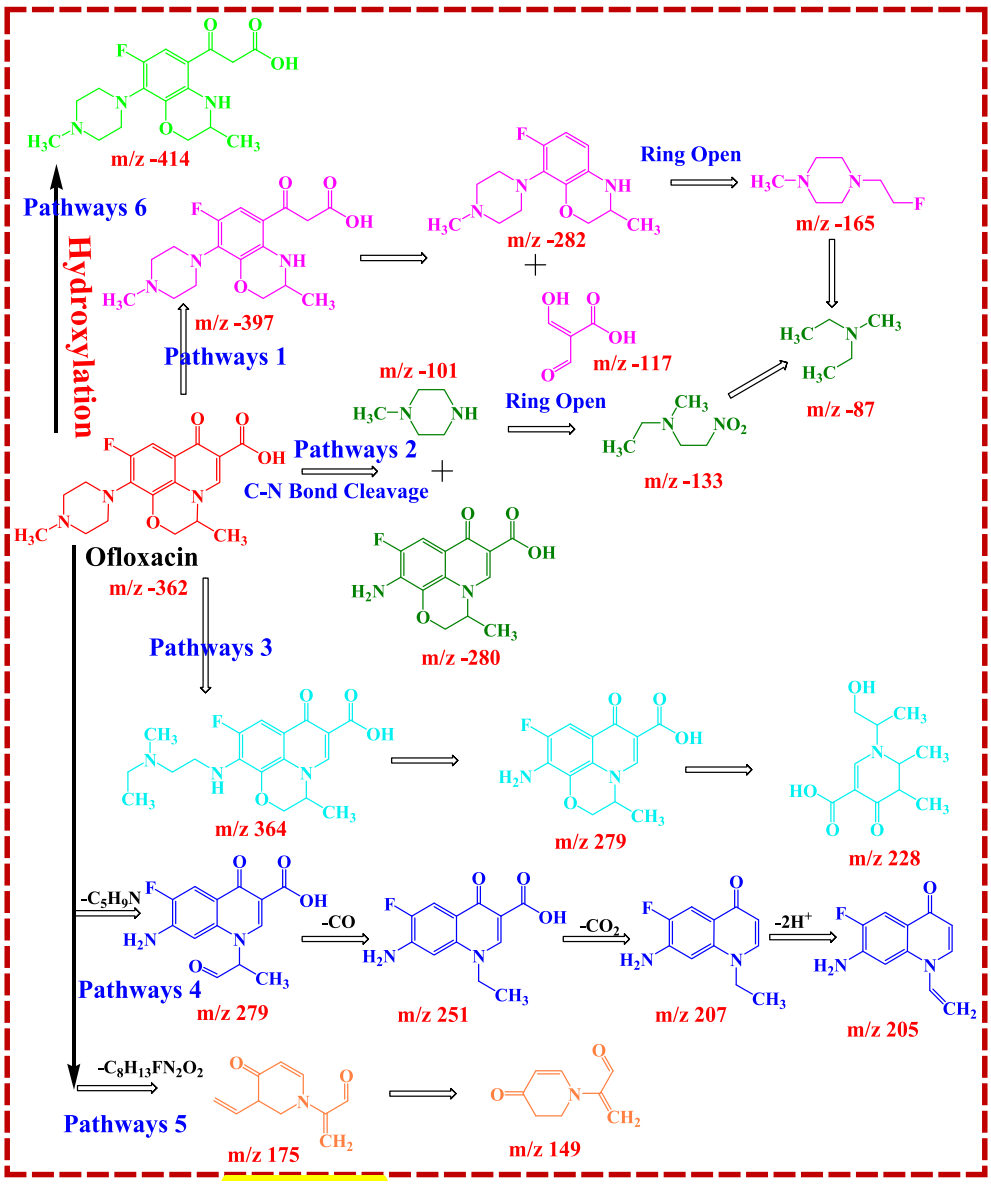

Fig. 8. Proposed reaction pathways for ofloxacin degradation in $LaCoO_3$/PMS system.

After each cycle of experiments, used catalyst was filtered by centrifugal separation, and then rinsed several times with Millipore water subsequently dried at 120 °C for 12 h. In order to collect the adequate amount of catalyst used for the next cycle, several parallel runs were conducted. The regenerated catalyst was further utilized at the same optimum operating conditions resulting in minor losses of ofloxacin and COD degradation was observed. The removal efficiency of ofloxacin significantly dropped from 97.11 % (1st cycle) to 94.08 %, 91.25 % and 90.12 %; and for COD removal 79.41 % (first cycle) to 76.29 %, 74.62 % and 70.31 %; in 2nd, 3rd and 4th successive cycles. Authors Liu et al., noticed the moxifloxacin removal in the five consecutive experiment cycles as 97.12 %, 97.13 %, 88.72 %, 80.43 %, and 62.63 %, respectively with $CoFe_2O_4$ catalyst activated with PMS [69]. The removal efficiency of ofloxacin and COD slightly suppressed in each cycle might be attributed to various reasons as: (**a**) leaching of cobalt ion leads to suppressed the active sites (Co^{+2}/Co^{+3}) from $LaCoO_3$ surface, and (**b**) carbon adsorbed on the catalyst surface and occupied the active sites (carbon in the form of intermediate compounds produced during the reaction) that causes blockage of active sites resulting in suppression of ROS species ($SO_4^{\bullet-}$ and $^{\bullet}OH$) production [31,34,77]. Furthermore, based on the XRD patterns obtained in Fig. 1(b), no significant changes were observed in spectral peaks of fresh and spent $LaCoO_3$ catalyst. This showed that catalyst $LaCoO_3$ is a highly stable structure. Considering the preceding facts, stability of $LaCoO_3$ perovskite was monitoring in term of cobalt ions leaching over each successive cycle through ICP-MS analysis as results shown in Fig. 5(e), supplementary file (Table S3). Leaching of Co ions in first cycle was noticed 1.64 mg/L, subsequently gradually dropped from 1.64 to 1.56, 1.18, and 0.98 mg/L in 2nd, 3rd and 4th successive cycle. However, the present values of Co ions leaching in each cycle were quite low which is in accordance with the permissible discharge limit in India [78,79]. Metal ions leaching is one of the primary drawbacks of heterogeneous catalyst, catalyst easily deactivate by losing the active sites from catalyst surface resulting in deteriorate the performance of catalyst. However, perovskite is a highly stable structure that doesn't lose its catalytic activity easily while using after recycling in multiple cycles [19,23]. Author Taran et al., tested the catalytic activity of $LaBO_3$ (B = Fe, Cu, Mn, Ni, Co) perovskite catalysts on phenol degradation and noticed that perovskite $LaFeO_3$ doesn't lost its catalytic activity after recycling over the forty cycles [23]. Similarly, authors Nie et al., tested the stability of $LaFeO_3$ perovskite-like catalyst for

sulfamethoxazole degradation and reported minor effects on sulfamethoxazole degradation efficiency after tenth cycle, along with low metal ions leaching [41]. It is noticeable that solution pH is strongly affected the chemical stability [23,31,77,80]. Meanwhile, leaching of Co ions on $LaCoO_3$ surface were evaluated at different pHs (i.e., 2.5, 5, 7.3, 10) at the same optimum operating conditions as shown in Fig. 5(f). Leaching of cobalt ions significantly decreased i.e., 2.33, 2.13, 1.64 and 1.60 mg/L with raising the reaction pHs (2.5, 5, 7.3, 10) with their corresponding removal efficiency of ofloxacin (56.35 %, 86.25 %, 97.11 % and 78.32 %) and COD (39.26 %, 63.26 %, 79.41 % and 51.36 %), respectively. Furthermore, the leaching of cobalt ions in a strong acidic medium was higher compared to pH 2.5, as well as very low removal of ofloxacin and COD was observed. Our previous study also found similar results, copper ion leaching gradually decreased 2.78, 2.24, 1.85, and 1.22 mg/L; and for nickel ion decreased gradually 1.65, 1.42, 1.26, and 1.08 mg/L; with raising in corresponding pHs 2, 4, 6.12 and 9, respectively catalysis with $SrCu_{0.6}Ni_{0.4}O_3$ perovskite-like catalyst [39]. Similarly, authors Qin et al. noticed very high leaching of iron ions in strong acidic medium e.g., 2.12 %, 1.88 %, 1.65 % and 1.28 %, at various pHs 2.1, 3.8, 5.8 and 10.2, respectively in Fe/ACP system for the removal of benzoic acid [77]. There have been several studies that have demonstrated very high metal ions leaching in strong acidic medium, which can be suppressed by raising the pH, along with improved the pollutant removal efficiency [77,80,81]. Thus, the above results demonstrate that stability and activity of the catalyst could be enhanced by conducting the degradation reaction in neutral and mild alkaline pH.

4. Ofloxacin and COD degradation kinetics

The degradation of ofloxacin and COD with $LaCoO_3$/PMS system was performed by two-stage degradation kinetics i.e., rapid degradation followed by slower degradation kinetics and well fitted by pseudo first order kinetic model at temperatures ranging 303 K to 343 K, as shown in Fig. 6(a, b). Various researchers have earlier explored the two-stage degradation pseudo first order kinetic model for different types of pollutants viz., pyridine, acrylonitrile, acrylamide and quinoline etc., [39,46,58,82]. Ofloxacin and COD degradation model is expressed by following Eq. (29).

$$rate = -\frac{dC}{dt} = kC^{p}C_{w}^{q} \tag{29}$$

Where, notation C is residual concentration of ofloxacin or COD in mg/L at time t, Cw is first order reaction rate constant (min^{-1}). Notation, p and q are the reaction order for ofloxacin catalyst dose. During the degradation reaction catalyst was not consumed, therefore term C_w could be neglected and applied p = 1 (for pseudo first order) and then Eq. (29) can be integrated and obtained following Eq. (30).

$$\ln\frac{C_o}{C_t} = kt \tag{30}$$

Fig. 6(a), depicted that degradation of ofloxacin with $LaCoO_3$/PMS system exhibited the bilinear plots, i.e., fast reaction for the initial 40 min duration (fast stage) followed by a slow reaction for the next 20 min reaction (slow stage). It is noticed that value of rate constants for ofloxacin and COD degradation increased with increasing the reaction temperature in both stage (fast stage k_1 as well as slower k_2). Meanwhile, value of rate constant in fast stage k1 was much higher than k_2 as tabulated in Table 3. Furthermore, the activation energy for ofloxacin

Table 3
Two-step degradation kinetics for ofloxacin and COD removal at various temperatures.

Temperature (K)	Fast Step			Slow Step		
	k_1 (min^{-1})	R^2	E_a (kJ mol^{-1})	k_2 (min^{-1})	R^2	E_a (kJ mol^{-1})
Ofloxacin degradation kinetics						
303	20.3 × 10^{-3}	0.973	28.60	7.3 × 10^{-3}	0.909	44.05
313	35.1 × 10^{-3}	0.990		11.6 × 10^{-3}	0.990	
323	48.6 × 10^{-3}	0.996		24.8 × 10^{-3}	0.983	
333	68.9 × 10^{-3}	0.997		44.7 × 10^{-3}	0.991	
343	76.4 × 10^{-3}	0.993		47.0 × 10^{-3}	0.999	
COD degradation kinetics						
303	14.7 × 10^{-3}	0.984	12.55	5.8 × 10^{-3}	0.998	19.37
313	20.5 × 10^{-3}	0.997		7.4 × 10^{-3}	0.984	
323	26.9 × 10^{-3}	0.996		8.8 × 10^{-3}	0.896	
333	33.2 × 10^{-3}	0.981		10.3 × 10^{-3}	0.961	
343	35.2 × 10^{-3}	0.995		11.0 × 10^{-3}	0.968	

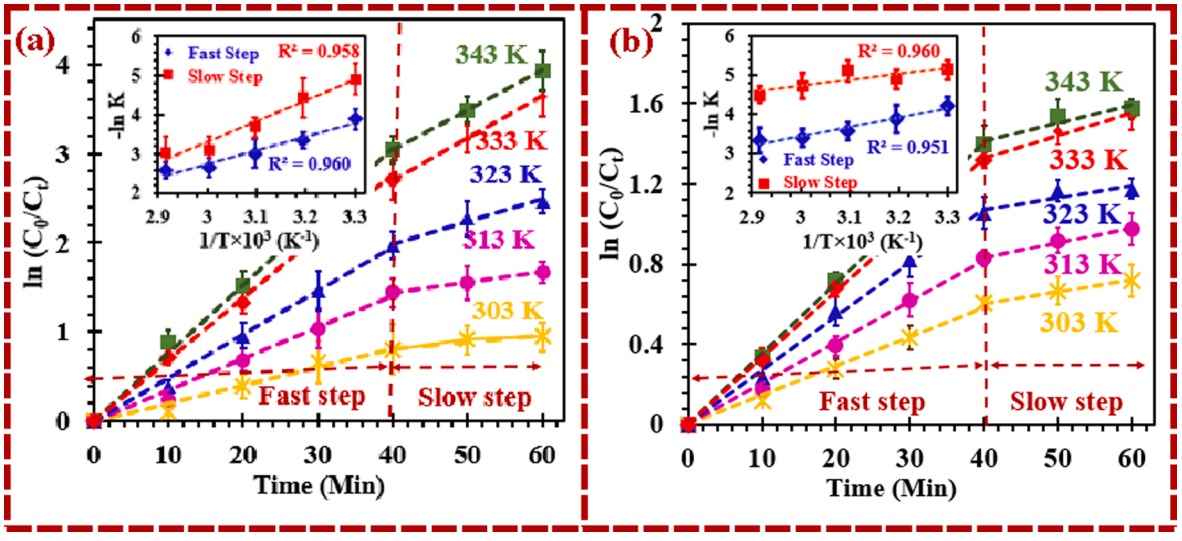

Fig. 6. Two-step degradation kinetics for (**a**) ofloxacin, and (**b**) COD removal at optimum operating conditions.

and COD degradation were estimated through Arrhenius equation by using rate constants k_1 and k_2. The values of activation energy for ofloxacin (i.e., 28.60 kJ mol^{-1} for fast stage and 44.05 kJ mol^{-1} for slow stage) and similarly for COD (i.e., 12.55 kJ mol^{-1} for fast stage and 19.37 kJ mol^{-1} for slow stage) degradation were obtained as shown in Table 3. Numerous researchers have reported the similar trends of activation energies for the degradation of various pollutants such as pyridine, pyrrole and quinoline to be 19.10, 41.29 and 29.40 kJ mol^{-1}, respectively [82–84].

5. Phytotoxicity study

Water generated from the industries contains the highly toxic and recalcitrant pollutants, which may adversely affect the growth of agricultural crops, either inhibited the growth of crops or delaying the germination of seeds [34,85,86]. As shown in Fig. 7 and supplementary file (Fig. S4), phytotoxicity experiments were conducted along with seed germination indices (G.I.) to evaluate the toxicity assessment of pharmaceutical wastewater on various plant species of *Vigna radiatus L., Cicer arietinum* and *Hordeum vulgare L.,* respectively. Various researchers have performed the phytotoxicity study and assessed the toxicity of industrial wastewater on various agricultural crops i.e., black chickpea [34], mustard [87], wheat, moong [34,88], some vegetables crops (e.g., tomato, chilli, onion and cucumber) [89], and subsequently results were reported that while using the high concentration toxic water in irrigation causes to detrimental impacts viz., crop growth inhibition, seed damaged and delaying in seed germination [90]. Therefore, considering the aforementioned facts, phytotoxicity tests were conducted with three species viz., *Vigna radiatus L.*, *Cicer arietinum* and *Hordeum vulgare L.,* germinating in control sample (tap water), untreated pharmaceutical wastewater and treated pharmaceutical wastewater, respectively. Prior to phytotoxicity test, seeds of each species were sterilized b soaking of 3 % H_2O_2 solution for 2 min and then rinsed several times in Millipore water [91]. All the experiments were carried out in duplicate and results were reported as mean average data. Duplicate samples of 10 seeds were utilized for each test. After 10 days of seeds germination, the germination index G.I. (%) was estimated through the following Eq. (31).

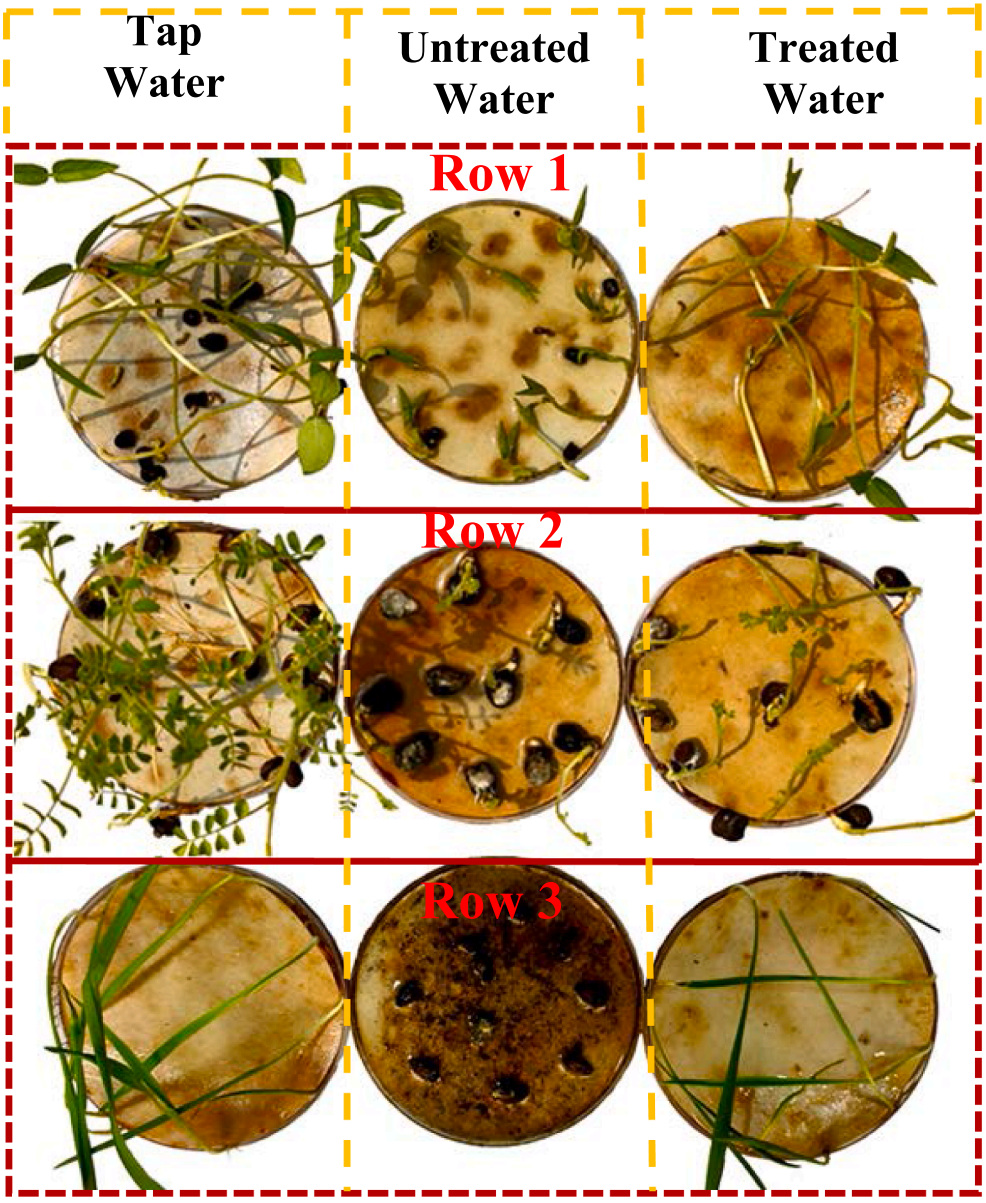

Fig. 7. Phytotoxicity assessment study with tap water, treated pharmaceutical manufacturing wastewater and untreated pharmaceutical manufacturing wastewater on species **Row** (1) Vigna radiatus L., **Row** (2) Cicer arietinum, and **Row** (3) Hordeum vulgare L.

$$G.I.(\%) = \frac{G_s}{G_c} \times \frac{L_s}{L_c} \times 100 \quad (31)$$

Where, notation Gs and Gc expressed as number of seeds germinated in sample water and control sample (tap water), Ls and Lc are value of root elongation (radical length) in sample water control sample. However, the values of G.I. (%) in pharmaceutical wastewater were assessed i.e., 20.24 %, 3.8 % and 0 % for species e.g., *Vigna radiatus L., Cicer arietinum* and *Hordeum vulgare L.,* respectively. Moreover, the values of G.I. (%) for *Vigna radiatus L., Cicer arietinum* and *Hordeum vulgare L.,* were estimated i.e., 63.24 %, 24.6 % and 80.36 % while germination of seed in treated pharmaceutical wastewater. However, G.I. (%) value lower than 50 % represent the highly phytotoxicity, intermediate values falling in the range 50–80 % represent the moderate phytotoxicity and values more than 80 % point out that material is non-toxic in nature for plant species. Similar ranges of G.I. (%) have been reported by authors Moradi and Ghanbari for plant species i.e., *Lycopersicum esculentum, Lepidium sativum* and *Raphanus sativus*, germinating in treated water from coagulation and Fenton process [86]. Additionally, the above results demonstrated that pharmaceutical wastewater strongly affects the growth of all plant species, but with a greater effect on *Hordeum vulgare L.* It might be cause of phytotoxins present in the wastewater [34,86,91]. As a result of the phytotoxicity results from our study, it was observed that a treatment with $LaCoO_3$/PMS system produced highly productive wastewater for Vigna radiatus L., Cicer arietinum and Hordeum vulgare L., respectively, despite having little impact on the above species.

6. Economic assessment of the treatment process

Implementing innovative technologies on a large scale has always been difficult due to the high cost of the treatment process. It is generally accepted that the total cost of the treatment process is the sum of the operating costs, capital costs, and investment costs [34,82]. The operating cost of heterogeneous catalysis with $LaCoO_3$/PMS system were estimated at lab scale for the real pharmaceutical manufacturing wastewater. The operating cost (in $/m^3$) included the chemical reagent cost and energy cost as shown in Table 4 [39,82]. The overall operating cost for pharmaceutical manufacturing wastewater was estimated to be 40.78$/m^3 wastewater with catalyst used in single cycle. The overall operating cost could be decreased in large scale operation and catalyst recycled in multiple cycles. In our previous research, treatment cost for real ABS resin wastewater was estimated 75.60$/m^3 with $LaCu_xFe_{1-x}O_3$/PMS system [34]. A study by Patidar and Srivastava, reported 209$/m^3 wastewater for electrochemical treatment of bulk drug pharmaceutical wastewater, which is a very high cost for real industrial wastewater treatment. The total cost of ofloxacin containing wastewater was reported 217.36$/m^3 by the sono-electrochemical process [7]. Similarly, other authors have reported the operating cost for real industrial wastewater as 436$/m^3 for highly acidic wastewater [92], 248$/m^3 for actual sugar industry wastewater [93], 217.36$/m^3 for cosmetic industry wastewater [85] and others have reported as given in Table S8 (supporting file). Thus, the above results concluded that the overall operating cost for pharmaceutical manufacturing wastewater with $LaCoO_3$/PMS system is very cost effective among the previously reported processes.

7. Conclusions

This study developed a highly efficient catalytic oxidation system to degrade ofloxacin and COD from pharmaceutical manufacturing wastewater. Catalyst $LaCoO_3$ exhibited excellent catalytic activity and stability toward PMS activation for ofloxacin degradation (97.11 %) and COD (79.41 %) under optimum operating conditions ($LaCoO_3$ dose 1 g/L, PMS 2 g/L, pH 7.32, and reaction temperature 60 °C). The two-stage degradation kinetics for ofloxacin and COD were performed by first order kinetic model at various temperatures 303–343 K. The activation energy for ofloxacin and COD degradation were estimated in fast stage 28.60 kJ/mol and 12.55 kJ/mol; and for slow stage 44.05 kJ/mol and 19.37 kJ/mol, respectively. Reusability and chemical stability studies of the catalyst revealed that ofloxacin and COD removal efficiency were only reduced by 7 % and 9 % over the fourth cycle, respectively. Furthermore, minor leaching of cobalt was observed i.e.,1.64, 1.54, 1.18 and 0.98 mg/L in 1st, 2nd, 3rd and 4th consecutive cycles, which was well below their respective possible limit prescribed by CBCB India, indicating that no secondary pollution is generated. The results of the quenching tests and EPR analysis confirmed the generation of massive ROS in $LaCoO_3$/PMS system, which provides superior performance in the removal of ofloxacin and COD. Six major reaction pathways for ofloxacin degradation were elucidated by intermediates and final products detected by GC-MS analysis. Phytotoxicity study demonstrated that the toxicity of pharmaceutical wastewater was significantly reduced and rate of seed germination highly improved after treatment. Furthermore, the treatment cost for ofloxacin degradation in $LaCoO_3$/PMS system was estimated to be very cost effective at 40.78$/m^3 of wastewater.

Table 4
Operating cost estimation for pharmaceutical manufacturing wastewater in $LaCoO_3$/PMS system.

Reagent	Chemical reagent cost for catalyst synthesis	
	Per unit price	Reagent cost for per g of catalyst
Lanthanum (III) nitrate hexahydrate	1110 ₹/kg	0.555₹/0.5 g
Cobalt (III) nitrate trihydrate	615₹/kg	0.307₹/0.5 g
Polyvinylpyrrolidone	350₹/kg	0.003₹/0.01 g
Citric acid	85₹/kg	0.085₹/1.0 g
Catalyst cost per g		0.950₹/g or 0.011$/g
Catalyst cost for optimum dose (1 g/L)		0.950₹/g or 0.011$/g

Reagent	Running cost of catalytic oxidation process		
	Price per unit	Cost for each run	Cost for 1 L
Peroxymonosulfate (PMS)	760₹/kg	0.152₹	1.52₹/2 g
Power consumption	5.65₹/kWh	0.086₹	0.860₹/h
Total operating cost per liter solution			3.33₹ or 0.0407$
Total operating cost per m^3 solution			3330₹ or 40.78$

Note: 1$ = 81.65 Indian Rupee as on November 11, 2022.

CRediT authorship contribution statement

Arvind Kumar: Conceptualization, Methodology, Investigation, Software, Data curation, Writing – original draft. **Basheswar Prasad:** Validation, Data curation, Visualization, Supervision. **Sheena Kumari:** Visualization, Supervision. **Faizal Bux:** Visualization, Data curation, Validation, Supervision.

Declaration of Competing Interest

The authors declare that they have no known competing financial interests or personal relationships that could have appeared to influence the work reported in this paper.

Data availability

Data will be made available on request.

Appendix A. Supplementary material

Supplementary data to this article can be found online at https://doi.org/10.1016/j.seppur.2023.123967.

References

[1] P. Gao, X. Tian, W. Fu, Y. Wang, Y. Nie, C. Yang, Y. Deng, Copper in $LaMnO_3$ to promote peroxymonosulfate activation by regulating the reactive oxygen species in sulfamethoxazole degradation, J. Hazard. Mater. 411 (2021), 125163.

[2] R. Changotra, H. Rajput, J. Paul Guin, L. Varshney, A. Dhir, Hybrid coagulation, gamma irradiation and biological treatment of real pharmaceutical wastewater, Chem. Eng. J. 370 (2019) 595–605.

[3] C. Nannou, A. Ofrydopoulou, E. Evgenidou, D. Heath, E. Heath, D. Lambropoulou, Antiviral drugs in aquatic environment and wastewater treatment plants: A review on occurrence, fate, removal and ecotoxicity, Sci. Total Environ. 699 (2020), 134322.

[4] L. Fang, K. Liu, F. Li, W. Zeng, Z. Hong, L. Xu, Q. Shi, Y. Ma, New insights into stoichiometric efficiency and synergistic mechanism of persulfate activation by zero-valent bimetal (Iron/Copper) for organic pollutant degradation, J. Hazard. Mater. 403 (2021), 123669.

[5] S. Karim, S. Bae, D. Greenwood, K. Hanna, N. Singhal, Degradation of 17α-ethinylestradiol by nano zero valent iron under different pH and dissolved oxygen levels, Water Res. 125 (2017) 32–41.

[6] R. Changotra, H. Rajput, A. Dhir, Treatment of real pharmaceutical wastewater using combined approach of Fenton applications and aerobic biological treatment, J. Photochem. Photobiol. A Chem. 376 (2019) 175–184.

[7] R. Patidar, V.C. Srivastava, Mechanistic insight into ultrasound-induced enhancement of electrochemical oxidation of ofloxacin: Multi-response optimization and cost analysis, Chemosphere. 257 (2020), 127121.

[8] Q. Su, J. Li, H. Yuan, B. Wang, Y. Wang, Y. Li, Y. Xing, Visible-light-driven photocatalytic degradation of ofloxacin by g-C_3N_4/NH_2-MIL-88B(Fe) heterostructure: Mechanisms, DFT calculation, degradation pathway and toxicity evolution, Chem. Eng. J. 427 (2022), 131594.

[9] R. Patidar, V.C. Srivastava, Mechanistic and kinetic insights of synergistic mineralization of ofloxacin using a sono-photo hybrid process, Chem. Eng. J. 403 (2021), 125736.

[10] A. Kaur, G. Gupta, A.O. Ibhadon, D.B. Salunke, A.S.K. Sinha, S.K. Kansal, A Facile synthesis of silver modified ZnO nanoplates for efficient removal of ofloxacin drug in aqueous phase under solar irradiation, J. Environ. Chem. Eng. 6 (2018) 3621–3630.

[11] D. Zhang, J. Qi, H. Ji, S. Li, L. Chen, T. Huang, C. Xu, X. Chen, W. Liu, Photocatalytic degradation of ofloxacin by perovskite-type $NaNbO_3$ nanorods modified g-C3N4 heterojunction under simulated solar light: Theoretical calculation, ofloxacin degradation pathways and toxicity evolution, Chem. Eng. J. 400 (2020), 125918.

[12] B. Lai, Y. Zhou, P. Yang, Treatment of wastewater from acrylonitrile-butadiene-styrene (ABS) resin manufacturing by biological activated carbon (BAC), J. Chem. Technol. Biotechnol. 88 (2013) 474–482.

[13] H. Karimi-Maleh, A. Ayati, R. Davoodi, B. Tanhaei, F. Karimi, S. Malekmohammadi, Y. Orooji, L. Fu, M. Sillanpää, Recent advances in using of chitosan-based adsorbents for removal of pharmaceutical contaminants: A review, J. Clean. Prod. 291 (2021), 125880.

[14] E. Hapeshi, I. Fotiou, D. Fatta-Kassinos, Sonophotocatalytic treatment of ofloxacin in secondary treated effluent and elucidation of its transformation products, Chem. Eng. J. 224 (2013) 96–105.

[15] B. Tiwari, B. Sellamuthu, Y. Ouarda, P. Drogui, R.D. Tyagi, G. Buelna, Review on fate and mechanism of removal of pharmaceutical pollutants from wastewater using biological approach, Bioresour. Technol. 224 (2017) 1–12.

[16] D. Kanakaraju, B.D. Glass, M. Oelgemöller, Advanced oxidation process-mediated removal of pharmaceuticals from water: A review, J. Environ. Manage. 219 (2018) 189–207.

[17] Y.H. Shin, N.C. Shin, B. Veriansyah, J. Kim, Y.W. Lee, Supercritical water oxidation of wastewater from acrylonitrile manufacturing plant, J. Hazard. Mater. 163 (2009) 1142–1147.

[18] A. Kumar, B. Prasad, K.K. Garg, Efficiently degradation of acrylonitrile from aqueous solution by $La_{0.5}Ce_{0.5}MO_3$ (M = Fe, Cu and Co) perovskite-like catalyst: Optimization and reaction pathways, J. Water Process Eng. 36 (2020), 101314.

[19] S. Zhu, Y. Xu, Z. Zhu, Z. Liu, W. Wang, Activation of peroxymonosulfate by magnetic Co-Fe/SiO_2 layered catalyst derived from iron sludge for ciprofloxacin degradation, Chem. Eng. J. 384 (2020), 123298.

[20] F. Ghanbari, M. Moradi, Application of peroxymonosulfate and its activation methods for degradation of environmental organic pollutants: Review, Chem. Eng. J. 310 (2017) 41–62.

[21] J. Yan, J. Li, J. Peng, H. Zhang, Y. Zhang, B. Lai, Efficient degradation of sulfamethoxazole by the CuO@Al_2O_3 (EPC) coupled PMS system: Optimization, degradation pathways and toxicity evaluation, Chem. Eng. J. 359 (2019) 1097–1110.

[22] S. Lu, G. Wang, S. Chen, H. Yu, F. Ye, X. Quan, Heterogeneous activation of peroxymonosulfate by $LaCo_{1-x}Cu_xO_3$ perovskites for degradation of organic pollutants, J. Hazard. Mater. 353 (2018) 401–409.

[23] O.P. Taran, A.B. Ayusheev, O.L. Ogorodnikova, I.P. Prosvirin, L.A. Isupova, V. N. Parmon, Perovskite-like catalysts LaBO3 (B=Cu, Fe, Mn Co, Ni) for wet peroxide oxidation of phenol, Appl. Catal. B Environ. 180 (2016) 86–93.

[24] R. Zhang, Y. Wan, J. Peng, G. Yao, Y. Zhang, B. Lai, Efficient degradation of atrazine by $LaCoO_3$/Al_2O_3 catalyzed peroxymonosulfate: Performance, degradation intermediates and mechanism, Chem. Eng. J. 372 (2019) 796–808.

[25] S. Yang, M. Besson, C. Descorme, Catalytic wet air oxidation of formic acid over Pt/$Ce_xZr_{1-x}O_2$ catalysts at low temperature and atmospheric pressure, Appl. Catal. B Environ. 100 (2010) 282–288.

[26] F. Soumia, C. Petrier, Effect of potassium monopersulfate (oxone) and operating parameters on sonochemical degradation of cationic dye in an aqueous solution, Ultrason. Sonochem. 32 (2016) 343–347.

[27] J. Sharma, I.M. Mishra, D.D. Dionysiou, V. Kumar, Oxidative removal of bisphenol a by uv-c/peroxymonosulfate (pms): Kinetics, influence of co-existing chemicals and degradation pathway, Chem. Eng. J. 276 (2015) 193–204.

[28] M. Han, Z. Ma, W. Zhang, H. Wang, The influences of hexadecyl trimethyl ammonium bromide on lanthanum titanate photocatalyst for ofloxacin degradation, J. Sol-Gel Sci. Technol. 96 (2020) 480–488.

[29] P. Hu, H. Su, Z. Chen, C. Yu, Q. Li, B. Zhou, P.J.J. Alvarez, M. Long, Selective degradation of organic pollutants using an efficient metal-free catalyst derived from carbonized polypyrrole via peroxymonosulfate activation, Environ. Sci. Technol. 51 (2017) 43.

[30] J. Miao, J. Sunarso, X. Duan, W. Zhou, S. Wang, Z. Shao, Nanostructured Co-Mn containing perovskites for degradation of pollutants: Insight into the activity and stability, J. Hazard. Mater. 349 (2018) 177–185.

[31] S. Ben Hammouda, F. Zhao, Z. Safaei, V. Srivastava, D. Lakshmi Ramasamy, S. Iftekhar, S. kalliola, M. Sillanpää, Degradation and mineralization of phenol in aqueous medium by heterogeneous monopersulfate activation on nanostructured cobalt based-perovskite catalysts $ACoO_3$ (A = La, Ba, Sr and Ce): Characterization, kinetics and mechanism study, Appl. Catal. B Environ. 215 (2017) 60–73.

[32] K.Y.A. Lin, Y.C. Chen, Y.F. Lin, $LaMO_3$ perovskites (M=Co, Cu, Fe and Ni) as heterogeneous catalysts for activating peroxymonosulfate in water, Chem. Eng. Sci. 160 (2017) 96–105.

[33] H. Zhu, P. Zhang, S. Dai, Recent advances of lanthanum-based perovskite oxides for catalysis, ACS Catal. 5 (2015) 6370–6385.

[34] A. Kumar, B. Prasad, K.K. Garg, Enhanced catalytic activity of series $LaCu_xFe_{1-x}O_3$ (x = 0.2, 0.4, 0.6, 0.8) perovskite-like catalyst for the treatment of highly toxic ABS resin wastewater: Phytotoxicity study, parameter optimization and reaction pathways, Process Saf. Environ. Prot. 147 (2021) 162–180.

[35] M. Mori, Y. Itagaki, Y. Sadaoka, Effect of VOC on ozone detection using semiconducting sensor with $SmFe_{1-x}Co_xO_3$ perovskite-type oxides, Sens. Actuat. B Chem. 163 (2012) 44–50.

[36] J.-J. Xu, D. Xu, Z.-L. Wang, H.-G. Wang, L.-L. Zhang, X.-B. Zhang, Synthesis of perovskite-based porous $La_{0.75}Sr_{0.25}$ MnO_3 nanotubes as a highly efficient electrocatalyst for rechargeable lithium-oxygen batteries, Angew. Chemie Int. Ed. 52 (2013) 3887–3890.

[37] A. Weidenkaff, Preparation and application of nanostructured perovskite phases, Adv. Eng. Mater. 6 (2004) 709–714.

[38] V. Gupta, M. Rakesh, Catalytic Wet Peroxide Oxidation (CWPO) of 2-Hydroxy-benzoic acid and contaminated industrial effluent using $LnMO_3$(Ln= La or Pr and M= Fe or Fe-Co), J. Water Process Eng. 27 (2019) 58–66.

[39] A. Kumar, B. Prasad, Mechanistic approach of $SO4^{\bullet-}$/$^{\bullet}OH$ radical toward target pollutants degradation simultaneously enhanced activity and stability of perovskite-like catalyst $SrCu_xNi_{1-x}O_3$, Sep. Purif. Technol. 279 (2021), 119677.

[40] T.T.N. Phan, A.N. Nikoloski, P.A. Bahri, D. Li, Heterogeneous photo-Fenton degradation of organics using highly efficient Cu-doped $LaFeO_3$ under visible light, J. Ind. Eng. Chem. 61 (2018) 53–64.

[41] Y. Nie, L. Zhang, Y.Y. Li, C. Hu, Enhanced Fenton-like degradation of refractory organic compounds by surface complex formation of $LaFeO_3$ and H_2O_2, J. Hazard. Mater. 294 (2015) 195–200.

[42] X. Cheng, X. Huang, X. Wang, D. Sun, Influence of calcination on the adsorptive removal of phosphate by Zn-Al layered double hydroxides from excess sludge liquor, J. Hazard. Mater. 177 (2010) 516–523.

[43] S. Jiang, H. Zhang, Y. Yan, X. Zhang, Stability and deactivation of Fe-ZSM-5 zeolite catalyst for catalytic wet peroxide oxidation of phenol in a membrane reactor, RSC Adv. 5 (2015) 41269–41277.

[44] S. Muthu Prabhu, S. Meenakshi, Enriched fluoride sorption using chitosan supported mixed metal oxides beads: Synthesis, characterization and mechanism, J. Water Process Eng. 2 (2014) 96–104.

[45] B. Babić-Stojić, V. Jokanović, D. Milivojević, M. Požek, Z. Jagličić, D. Makovec, N. J. Orsini, M. Marković, K. Arsikin, V. Paunović, Ultra small iron oxide nanoparticles: Magnetic and NMR relaxometric properties, Curr. Appl. Phys. 18 (2018) 141–149.

[46] V. Gosu, A. Dhakar, P. Sikarwar, U.K.A. Kumar, V. Subbaramaiah, T.C. Zhang, Wet peroxidation of resorcinol catalyzed by copper impregnated granular activated carbon, J. Environ. Manage. 223 (2018) 825–833.

[47] J. Coates, Interpretation of Infrared Spectra, A Practical Approach, Encycl. Anal. Chem. (2006) 10815–10837.

[48] K. Karthik, S. Dhanuskodi, C. Gobinath, S. Prabukumar, S. Sivaramakrishnan, Multifunctional properties of microwave assisted CdO–NiO–ZnO mixed metal oxide nanocomposite: enhanced photocatalytic and antibacterial activities, J. Mater. Sci. Mater. Electron. 29 (2018) 5459–5471.

[49] D. Pan, S. Ge, J. Zhao, Q. Shao, L. Guo, X. Zhang, J. Lin, G. Xu, Z. Guo, Synthesis, characterization and photocatalytic activity of mixed-metal oxides derived from NiCoFe ternary layered double hydroxides, Dalt. Trans. 47 (2018) 9765–9778.

[50] R.R. Solís, F.J. Rivas, O. Gimeno, Removal of aqueous metazachlor, tembotrione, tritosulfuron and ethofumesate by heterogeneous monopersulfate decomposition on lanthanum-cobalt perovskites, Appl. Catal. B Environ. 200 (2017) 83–92.

[51] D. Mao, F. He, P. Zhao, S. Liu, Enhancement of resistance to chlorine poisoning of Sn-modified MnCeLa catalysts for chlorobenzene oxidation at low temperature, RSC Adv. 5 (2015) 10040–10047.

[52] K. Zhao, F. He, Z. Huang, A. Zheng, H. Li, Z. Zhao, Three-dimensionally ordered macroporous $LaFeO_3$ perovskites for chemical-looping steam reforming of methane, Int. J. Hydrogen Energy. 39 (2014) 3243–3252.

[53] C. Zhang, C. Wang, W. Hua, Y. Guo, G. Lu, S. Gil, A. Giroir-Fendler, Relationship between catalytic deactivation and physicochemical properties of $LaMnO_3$ perovskite catalyst during catalytic oxidation of vinyl chloride, Appl. Catal. B Environ. 186 (2016) 173–183.

[54] S. Maghsoodi, J. Towfighi, A. Khodadadi, Y. Mortazavi, The effects of excess manganese in nano-size lanthanum manganite perovskite on enhancement of trichloroethylene oxidation activity, Chem. Eng. J. 215–216 (2013) 827–837.

[55] Y. Feng, P.H. Lee, D. Wu, K. Shih, Surface-bound sulfate radical-dominated degradation of 1,4-dioxane by alumina-supported palladium (Pd/Al_2O_3) catalyzed peroxymonosulfate, Water Res. 120 (2017) 12–21.

[56] F. Jiang, B. Qiu, D. Sun, Advanced degradation of refractory pollutants in incineration leachate by UV/Peroxymonosulfate, Chem. Eng. J. 349 (2018) 338–346.

[57] Y. Bao, W. Da Oh, T.T. Lim, R. Wang, R.D. Webster, X. Hu, Elucidation of stoichiometric efficiency, radical generation and transformation pathway during catalytic oxidation of sulfamethoxazole via peroxymonosulfate activation, Water Res. 151 (2019) 64–74.

[58] S. Singh, S.L. Lo, Catalytic performance of hierarchical metal oxides for per-oxidative degradation of pyridine in aqueous solution, Chem. Eng. J. 309 (2017) 753–765.

[59] Z. Wu, Y. Wang, Z. Xiong, Z. Ao, S. Pu, G. Yao, B. Lai, Core-shell magnetic Fe_3O_4@Zn/Co-ZIFs to activate peroxymonosulfate for highly efficient degradation of carbamazepine, Appl. Catal. B Environ. 277 (2020), 119136.

[60] Z. Yang, Y. Li, X. Zhang, X. Cui, S. He, H. Liang, A. Ding, Sludge activated carbon-based $CoFe_2O_4$-SAC nanocomposites used as heterogeneous catalysts for degrading antibiotic norfloxacin through activating peroxymonosulfate, Chem. Eng. J. 384 (2020), 123319.

[61] A. Kumar, B. Prasad, V.K. Sandhwar, K.K. Garg, Mechanistic insight into heterogeneous Fenton-like catalysis with M-Al_2O_3/SiO_2(M = Fe, Co and Ni) for acrylonitrile mineralization from real ABS resin wastewater: Optimization and toxicity assessment, J. Environ. Chem. Eng. 9 (2021), 105177.

[62] L. Lai, J. Yan, J. Li, B. Lai, Co/Al_2O_3-EPM as peroxymonosulfate activator for sulfamethoxazole removal: Performance, biotoxicity, degradation pathways and mechanism, Chem. Eng. J. 334 (2018) 676–688.

[63] Z. Shen, H. Zhou, Z. Pan, Y. Guo, Y. Yuan, G. Yao, B. Lai, Degradation of atrazine by Bi_2MoO_6 activated peroxymonosulfate under visible light irradiation, J. Hazard. Mater. 400 (2020), 123187.

[64] Y. Hong, J. Peng, X. Zhao, Y. Yan, B. Lai, G. Yao, Efficient degradation of atrazine by CoMgAl layered double oxides catalyzed peroxymonosulfate: Optimization, degradation pathways and mechanism, Chem. Eng. J. 370 (2019) 354–363.

[65] J. Cao, L. Lai, B. Lai, G. Yao, X. Chen, L. Song, Degradation of tetracycline by peroxymonosulfate activated with zero-valent iron: Performance, intermediates, toxicity and mechanism, Chem. Eng. J. 364 (2019) 45–56.

[66] J. Wang, S. Wang, Activation of persulfate (PS) and peroxymonosulfate (PMS) and application for the degradation of emerging contaminants, Chem. Eng. J. 334 (2018) 1502–1517.

[67] P. Liang, D. Meng, Y. Liang, Z. Wang, C. Zhang, S. Wang, Z. Zhang, Cation deficiency tuned $LaCoO_{3-\delta}$ perovskite for peroxymonosulfate activation towards bisphenol A degradation, Chem. Eng. J. 409 (2021), 128196.

[68] Y. Hong, H. Zhou, Z. Xiong, Y. Liu, G. Yao, B. Lai, Heterogeneous activation of peroxymonosulfate by CoMgFe-LDO for degradation of carbamazepine: Efficiency, mechanism and degradation pathways, Chem. Eng. J. 391 (2020), 123604.

[69] L. Liu, H. Mi, M. Zhang, F. Sun, R. Zhan, H. Zhao, S. He, L. Zhou, Efficient moxifloxacin degradation by $CoFe_2O_4$ magnetic nanoparticles activated peroxymonosulfate: Kinetics, pathways and mechanisms, Chem. Eng. J. 407 (2021), 127201.

[70] M.F. Sunding, K. Hadidi, S. Diplas, O.M. Løvvik, T.E. Norby, A.E. Gunnæs, XPS characterisation of in situ treated lanthanum oxide and hydroxide using tailored charge referencing and peak fitting procedures, J. Electron Spectros. Relat. Phenomena. 184 (2011) 399–409.

[71] Y. Pang, X. Zhou, E.I. Vovk, C. Guan, S. Li, A.P. van Bavel, Y. Yang, Understanding lanthanum oxide surface structure by DFT simulation of oxygen 1s calibrated binding energy in XPS after in situ treatment, Appl. Surf. Sci. 548 (2021), 149214.

[72] C. Su, X. Duan, J. Miao, Y. Zhong, W. Zhou, S. Wang, Z. Shao, Mixed conducting perovskite materials as superior catalysts for fast aqueous-phase advanced oxidation: A Mechanistic Study, ACS Catal. 7 (2017) 388–397.

[73] J. Li, M. Xu, G. Yao, B. Lai, Enhancement of the degradation of atrazine through $CoFe_2O_4$ activated peroxymonosulfate (PMS) process: kinetic, degradation intermediates, and toxicity evaluation, Chem. Eng. J. 348 (2018) 1012–1024.

[74] M. Xu, H. Zhou, Z. Wu, N. Li, Z. Xiong, G. Yao, B. Lai, Efficient degradation of sulfamethoxazole by $NiCo_2O_4$ modified expanded graphite activated peroxymonosulfate: Characterization, mechanism and degradation intermediates, J. Hazard. Mater. 399 (2020), 123103.

[75] J. Jimenez-Villarin, A. Serra-Clusellas, C. Martínez, A. Conesa, J. Garcia-Montaño, E. Moyano, Liquid chromatography coupled to tandem and high-resolution mass spectrometry for the characterisation of ofloxacin transformation products after titanium dioxide photocatalysis, J. Chromatogr. A. 1443 (2016) 201–210.

[76] Y. Zhu, M. Wei, Z. Pan, L. Li, J. Liang, K. Yu, Y. Zhang, Ultraviolet/peroxydisulfate degradation of ofloxacin in seawater: Kinetics, mechanism and toxicity of products, Sci. Total Environ. 705 (2020), 135960.

[77] H. Qin, R. Xiao, J. Chen, Catalytic wet peroxide oxidation of benzoic acid over Fe/AC catalysts: Effect of nitrogen and sulfur co-doped activated carbon, Sci. Total Environ. 626 (2018) 1414–1420.

[78] Central Pollution Control Board (CPCB), Pollution control acts, and notification under CPCB, India (2012). https://www.cpcb.nic.

[79] A. Kumar, B. Prasad, K.K. Garg, Catalytic peroxidation of acrylic acid from aqueous solution incorporated with highly active $La_{0.5}Sr_{0.5}BO_3$ (B=Cu, Fe and Ni) perovskite-like catalysts, J. Environ. Heal. Sci. Eng. 18 (2020) 897–913.

[80] Y. Lei, C.S. Chen, Y.J. Tu, Y.H. Huang, H. Zhang, Heterogeneous degradation of organic pollutants by persulfate activated by CuO-Fe_3O_4: Mechanism, stability, and effects of pH and bicarbonate ions, Environ. Sci. Technol. 49 (2015) 6838–6845.

[81] S. Ben Hammouda, F. Zhao, Z. Safaei, I. Babu, D.L. Ramasamy, M. Sillanpää, Reactivity of novel Ceria-Perovskite composites CeO_2- $LaMO_3$ (MCu, Fe) in the catalytic wet peroxidative oxidation of the new emergent pollutant 'Bisphenol F': Characterization, kinetic and mechanism studies, Appl. Catal. B Environ. 218 (2017) 119–136.

[82] V. Subbaramaiah, V.C. Srivastava, I.D. Mall, Catalytic wet peroxidation of pyridine bearing wastewater by cerium supported SBA-15, J. Hazard. Mater. 248–249 (2013) 355–363.

[83] S. Garg, V.C. Srivastava, S. Singh, T.K. Mandal, Catalytic degradation of pyrrole in aqueous solution by Cu/SBA-15, Int. J. Chem. React. Eng. 13 (2015) 437–445.

[84] N.J. Pachupate, P.D. Vaidya, Catalytic wet oxidation of quinoline over Ru/C catalyst, J. Environ. Chem. Eng. 6 (2018) 883–889.

[85] R. Patidar, V.C. Srivastava, Ultrasound Enhanced Electro-Fenton Mineralization of Benzophenone: Kinetics and Mechanistic Analysis, ACS ES T, Water. (2022).

[86] M. Moradi, F. Ghanbari, Application of response surface method for coagulation process in leachate treatment as pretreatment for Fenton process: Biodegradability improvement, J. Water Process Eng. 4 (2014) 67–73.

[87] S. Mazhar, A. Ditta, L. Bulgariu, I. Ahmad, M. Ahmed, A.A. Nadiri, Sequential treatment of paper and pulp industrial wastewater: Prediction of water quality parameters by Mamdani Fuzzy Logic model and phytotoxicity assessment, Chemosphere. 227 (2019) 256–268.

[88] P.K. Singh, K. Ladwani, K. Ladwani, P.B. Deshbhratar, D.S. Ramteke, Impact of paper mill wastewater on soil properties and crop yield through lysimeter studies, Environ. Technol. 34 (2013) 599–606.

[89] S. Ramana, A.K. Biswas, S. Kundu, J.K. Saha, R.B.R. Yadav, Effect of distillery effluent on seed germination in some vegetable crops, Bioresour. Technol. 82 (2002) 273–275.

[90] R.I. Khaleel, N. Ismail, M.H. Ibrahim, The Impact of waste water treatments on seed germination and biochemical parameter of Abelmoschus Esculentus L, Procedia - Soc, Behav. Sci. 91 (2013) 453–460.

[91] B. Ravindran, S.K.S. Kumari, T.A. Stenstrom, F. Bux, Evaluation of phytotoxicity effect on selected crops using treated and untreated wastewater from different configurative domestic wastewater plants, Environ. Technol. (United Kingdom) 37 (2016) 1782–1789.

[92] A. Goyal, V.C. Srivastava, J.P. Kushwaha, Treatment of highly acidic wastewater containing high energetic compounds using dimensionally stable anode, Chem. Eng. J. 325 (2017) 289–299.

[93] O.P. Sahu, V. Gupta, P.K. Chaudhari, V.C. Srivastava, Electrochemical treatment of actual sugar industry wastewater using aluminum electrode, Int. J. Environ. Sci. Technol. 12 (2015) 3519–3530.